Leveraging L_3 to Transfer to L_4 in the Sun-perturbed Earth-Moon System

Yuying Liang*, [1], Begoña Nicolás [2] and Àngel Jorba [2]

[1] Department of Earth and Space Science and Engineering, York University, Toronto, M3J1P3, Canada

[2] Departament de Matemàtiques i Informàtica, Universitat de Barcelona, Barcelona, 08007, Spain

* e: buaa_liangyuying@163.com

Abstract: This paper is devoted to a new approach to construct the transfers from the Earth to the Earth-Moon (EM) L_4 using stable and unstable manifolds of quasi-periodic Lyapunov orbits (QPLOs) of the EM L_3 in the planar bicircular Sun-Earth-Moon system. Some QPLOs have stable manifolds intersecting the Earth parking orbits and unstable manifolds going through the EM L_4 region, which gives a skeleton to build up such transfers. Tentatively, the stable and unstable manifolds of a QPLO are employed to construct transfer segments connecting the Earth and L_4 vicinity, respectively. The trajectories near the stable manifolds spent some time moving around L_3 before going away and approaching the unstable manifolds towards L_4. To reduce the multi-revolution behavior around L_3, a multiple shooting algorithm is developed to switch from the stable to the unstable manifold, where additional maneuvers are performed at some distance from the QPLO to reduce the time spent in the L_3 vicinity. By such construction a spacecraft can visit and park around two high-cost far-away libration points in a single journey. Eliminating most of the loops around L_3, the quickest one among the example transfers needs about 175 days. Furthermore, it is showed how to utilize the stable manifolds of the QPLO alone to design faster transfers to the EM L_4 vicinity. By this construction, the lowest time of flight is about 61 days. The advantages of these two constructions are discussed.

Keywords: Transfer to Triangular Libration Points, Bi-circular Problem, L_3 Libration Point, Multiple Shooting Algorithm, Computation of Invariant Tori

1. Introduction

1.1 Role of Triangular Libration Points in Space Applications

The dynamics near the triangular libration points is a classical problem in the field of celestial mechanics, initially motivated by the discovery of Trojan asteroids [1]. Due to the unique geometric location of triangular libration points with respect to both the Earth and the Moon, Maccone first proposed that L_4 could be used for planetary defence and L_5 for Moon farside exploration [2]. Liang et al. demonstrated that the region near the Earth-Moon triangular libration points is a perfect reservation place for asteroid capture mission [3]. Furthermore, the very long distance between a triangular libration point probe and a ground station, or between two triangular libration point probes, can aid very long baseline interferometry and can greatly enhance the accuracy of the observations [4]. Recently, the concept of a space weather mission is put forward and being studied in the framework of the European Space Agency's Space Situational Awareness Program, where a spacecraft is envisioned to be placed at the Sun-Earth L_5 point for the purpose of solar wind surveillance [5]. With the increasing capability of advanced high-impulse thrusters, e.g., magneto-plasma dynamic thrusters tested in laboratories for thrust up to 200 N [6],

deep space exploration to the vicinity of triangular libration points can be achieved at the expense of affordable fuel consumption. Therefore, the triangular libration points is playing a very important role in future space exploration.

To serve future remote sensing or observation missions, the existence of natural formation flying trajectories near the Earth-Moon triangular libration points were first investigated by Catlin and McLaughlin [7]. Salazar et al. explored the relative radial acceleration with respect to a nominal trajectory near the triangular libration points in the circular restricted three-body problem (CR3BP) [8], and then in the bi-circular problem (BCP) considering solar gravity perturbation [9]. In the real force model, the instability near triangular libration points is much milder than the one near collinear libration points [10]. As a result, a much lower station keeping frequency should be expected [11].

1.2 Transfers to the Earth-Moon and Sun-Earth Triangular Libration Points

To achieve these targets, most of the literature on triangular libration points from the field of astrodynamics are devoted to the construction of transfers to the Earth-Moon or Sun-Earth triangular libration points. Salazar et al. proposed a design method for transfers from Earth-bound elliptic trajectories to the Earth-Moon triangular libration points by exploiting the chaotic region that connects the Earth with the Moon [12]. By matching the lunar gravity assist segments and the stable manifolds of a cislunar resonant orbit, Lei and Xu designed low-energy transfers to the triangular libration points of the Earth-Moon system [13]. Similarly, Vaquero and Howell successfully constructed transfers to many typical libration periodic orbits (LPOs) including those near triangular libration points via the patching of invariant manifolds of resonant orbits in the Earth-Moon CR3BP and transitioned the results to an ephemeris model [14]. Targeting at the triangular libration points in the Earth-Moon system, Zhao and Hou proposed two feasible transfer mechanisms using lunar and solar gravity assists, respectively, and showed that the theoretical minimum fuel consumption is 3.0975 km/s for transfers from a 200 km altitude Earth parking orbit in the Earth-Moon CR3BP system [11]. All the aforementioned transfers require at least two maneuvers, one for speed-up to escape from the Earth gravity field and the other for speed-down to approach the triangular libration point vicinity. Whereas Tan et al. creatively developed a single impulsive strategy to transfer a spacecraft from the Earth to the Earth-Moon L_4 based on differential correction [15]. Instead of impulsive thrust, transfers to triangular libration points by a low-thrust technique are also investigated by many scholars. Taking advantage of the invariant manifolds of LPOs in the CR3BP, Elliott et al. [16] and Sullivan et al. [17] designed a low-thrust-enabled trajectory to the Sun-Earth $L5$ region. Based on the horseshoe orbits encircling triangular libration points and L_3, the pseudospectral method and the tangential thrust control strategy are introduced to optimize two kinds of trajectories from the Earth to Earth-Moon triangular libration points, respectively [18]. The low-thrust fuel-optimal transfers from Halo orbits to periodic orbits around Earth-Moon triangular libration points are obtained by an indirect optimization technique incorporated with constraint gradients [19]. Furthermore, different from the Earth-Moon or Sun-Earth systems, Trivailo discussed a new scenario where a spacecraft is located near triangular libration points in a Sun-planet system under perturbation of multiple Trojan asteroids [20]. He showed that under such circumstances the minimum thrust for the optimized transfer trajectories from L_4 to L_5 is vastly different to that from L_5 to L_4.

1.3 Dynamical Connection of Triangular Libration Points and L_3

The triangular libration points have a strong dynamical connection to L_3 from many aspects. In the framework of the CR3BP, the triangular libration points are surrounded by planar families of long- and short-period periodic orbits and a vertical family of periodic orbits as $\mu < \mu_R$ [21]. From a bifurcation point along the short-period family of the equilateral points emerges a planar Lyapunov orbit around L_3 and the vertical periodic orbit family around the triangular libration points connects to the vertical Lyapunov family around L_3 [22, 23]. At quite small μ, the practical stability domain around the triangular libration points is slightly outside the zero-velocity curve on the energy level of L_3 and the reason leading to the escape of a spacecraft from this domain is the passage close to L_3 [24]. The horseshoe orbits that grow from L_3 towards the secondary body extend through a vast area, approaching the vicinity of the triangular libration points, L_4 and L_5. This has been shown for a wide range of CR3BP mass ratios [25]. In the framework of the CR3BP, Anderlecht explored the links between Tadpole orbits around the triangular libration points to other families of LPOs, including Lyapunov orbits around L_3 [26]. As the dynamical model is upgraded from CR3BP to Third-body perturbed model, e.g., Bi-circular Problem (BCP), some of the dynamical connections of triangular libration points and L_3 remain, such as the horseshoe orbits, which suggests an alternative approach to transfer to triangular libration points through L_3.

For the first time, this investigation shows how to leverage the stable/unstable manifolds of quasi-periodic libration orbits (QPLOs) around L_3 to construct transfer orbits from a circular Earth parking orbit to a quasi-periodic orbit around the Earth-Moon triangular libration points considering solar gravity perturbation. The first construction successfully builds up transfer trajectories by patching stable and unstable manifolds of QPLOs around L_3 and such transfers enable a spacecraft visit both L_3 and L_4 points in a single journey. The total time of flight (TOF) highly depends on the multi-revolutions around L_3 and becomes adjustable and flexible to satisfy the mission requirements by various combination of the stable and unstable manifolds segments of QPLOs. The smooth connections between them are numerically validated by multiple shooting method at a compensation of quite a small amount of fuel consumption. Thus, the transfers carried out by the first construction of this investigation have potential to join up with an L_3-encircling mission as an extended task. However, the total TOF is quite long even eliminating most of the revolutions around L_3. Then, a second construction is proposed only using the stable manifolds of QPLOs that connect both a circular Earth parking orbit and the Earth-Moon L_4 vicinity together. For missions avoiding to visit L_3, the total TOF can be further decreased to 61 days.

In this investigation, the BCP is utilized to model the effect of the solar gravity as a periodic time-dependent perturbation of the CR3BP (see **Section 2**). In this model, the Earth-Moon libration points are replaced by periodic orbits. In particular, triangular libration points are replaced by three short-period periodic orbits [27] with quasi-periodic orbit motion around them [28, 29]. The stability of the triangular libration points is proved for any CR3BP with a mass ratio μ smaller than the Routh critical value μ_R, except for some resonance cases [30]. However, the situation changes when perturbations are taken into consideration, e.g., solar gravity [29], eccentricity of lunar orbit [31] and Earth's oblateness [32]. The very general way to deal with perturbed transfers in the Sun-Earth-Moon system is by refining the original trajectory in the CR3BP to higher-fidelity model e.g., [14, 33], or by decoupling the Sun-Earth-Moon-spacecraft four-body system into two coupled CR3BPs e.g., [34]. One benefit of decomposing the Sun-Earth-Moon-spacecraft four-body system into two coupled CR3BPs is to preserve the useful dynamical structure obtained in the CR3BP, e.g., invariant manifolds and LPOs. However, the ignored third-body gravity

perturbation, especially the dominant solar gravity over the lunar gravity in the area outsides lunar sphere of influence, has a remarkably large effect on the motion of a spacecraft in the Sun-Earth-Moon system far from both the Earth and the Moon, e.g., the transfers to triangular libration points. The Sun not only alters the stability of the Earth-Moon libration points themselves, but also gives birth to unique dynamical properties. Thus, this investigation adopts the implementation of dealing with the Sun-perturbed motion in a BCP model. In many situations, the BCP model is regarded as a good replacement of the real Sun-Earth-Moon system [29, 35].

This paper is organized as follows: in **Section 2**, a brief introduction of the dynamical model and the associated mathematical tools is given. **Section 3** is devoted to the construction of near-Earth and near-L_4 segments of the stable and unstable manifolds of a quasi-periodic Lyapunov orbit around L_3, respectively. In **Section 4**, a patching method based on the multiple shooting algorithm is developed to design and manage the looping segments of stable and unstable manifolds of quasi-periodic Lyapunov orbits around L_3 and some typical transfer trajectories are shown, where a special situation using only the stable manifolds of a quasi-periodic Lyapunov orbit around L_3 is discussed.

2. Dynamical Model and Mathematical Tools

2.1 Bi-circular Problem (BCP)

The well-known Circular Restricted Three-Body Problem (CR3BP) describes the movement of a massless particle subjected to the gravitational fields of two primary masses, referred to as m_1 and m_2 ($m_1 > m_2$). They are supposed to revolve counter-clockwise in circular motion around their common center of masses, taken as the origin of the frame. Five libration points are found in this model; the collinear points L_1, L_2 and L_3 are placed along the line connecting two primaries, the first two on both sides of the smaller primary and L_3 close to the opposite position of the smaller primary, and the triangular points L_4 and L_5 are placed at the third vertex of the equilateral triangles defined by taking the primaries as the other two vertices. From now on, L_1, L_2, L_3, L_4, and L_5 denote the libration points in the Earth-Moon system without any specification in this investigation.

Some modifications of the CR3BP have been developed over the years in order to define models that account for additional physical effects. Among them, the BCP adopted in this investigation introduces a time-periodic perturbation that corresponds to the gravitational field of a third massive body that only acts on the massless particle [36, 37]. In this investigation, the primaries are the Earth and Moon moving in a circular orbit around their common center of mass that is assumed to revolve around the Sun in a circular orbit. The Sun produces a periodic time-dependent forcing on the Earth-Moon CR3BP. Remark that under such assumptions, the motion of the three masses do not follow Newton's law. As this investigation concerns the motion near the Earth and the Moon, the Earth-Moon rotating frame, denoted as O-x-y, is introduced to set up the equations of motion of the spacecraft in this BCP. As shown in Fig. 1, the origin is located at the center of mass of Earth and Moon and the Earth and Moon are fixed on the horizontal axis at positions (μ, 0) and (μ-1, 0), where $\mu = \frac{m_2}{m_1 + m_2}$ and m_1 and m_2 denote the mass of the Earth and Moon, respectively. The x-axis lies along the line from the Moon to the Earth with the y-axis perpendicular to it, completing a right-handed coordinate system. Besides, the motions are considered and the transfers are constructed in the (x, y) plane in this investigation. As usual, the units of length, mass and time are the distance

between the primaries (384400 km), the sum of the masses of the Earth and Moon (6.0457×10^{24} kg) and that the period of their circular motion (27.31 days) is 2π units of time. In these units, the gravitational constant is 1.

With these considerations, given the coordinate (x, y) of a spacecraft, its motion in the planar BCP is described by the following equations

$$\begin{cases} \ddot{x}=2\dot{y}+x-(1-\mu)\frac{x-\mu}{r_{PE}^3}-\mu\frac{x+1-\mu}{r_{PM}^3}-m_S\frac{x-x_S}{r_{PS}^3}-m_S\frac{x_S}{a_S^3} \\ \ddot{y}=-2\dot{x}+y-(1-\mu)\frac{y}{r_{PE}^3}-\mu\frac{y}{r_{PM}^3}-m_S\frac{y-y_S}{r_{PS}^3}-m_S\frac{y_S}{a_S^3} \end{cases} \tag{1}$$

$$\begin{cases} r_{PE}^2=(x-\mu)^2+y^2 \\ r_{PM}^2=(x+1-\mu)^2+y^2 \\ r_{PS}^2=(x-x_S)^2+(y-y_S)^2 \end{cases} \tag{2}$$

where (x_s, y_s) is the position of the Sun in the Earth-Moon rotating frame,

$$\begin{cases} x_S=a_S\cos(\omega_S t+\theta_0) \\ y_S=-a_S\sin(\omega_S t+\theta_0) \end{cases} \tag{3}$$

In Eq. (1)-(3), r_{PS}, r_{PE} and r_{PM} denote the distance from the spacecraft to the Sun, the Earth and the Moon, respectively. m_S denotes the mass of the Sun and a_S denotes the distance between the Sun position and the Earth-Moon center of mass. ω_S is the solar angular velocity in the rotating (synodic) frame and θ_0 is the initial phase angle of the Sun measured from the positive x-axis of the Earth-Moon rotating frame. The values of these parameters are included in Table 1 in the normalized units. Note that, at the initial time $t=0$, the Sun is placed on the x-axis at $(a_s, 0)$, corresponding to a lunar eclipse.

Table 1 Normalized Parameters of the Sun-Earth-Moon system

μ	m_S	ω_S	a_S	θ_0
0.012150582	328900.54999	0.925195985	388.811143023	0
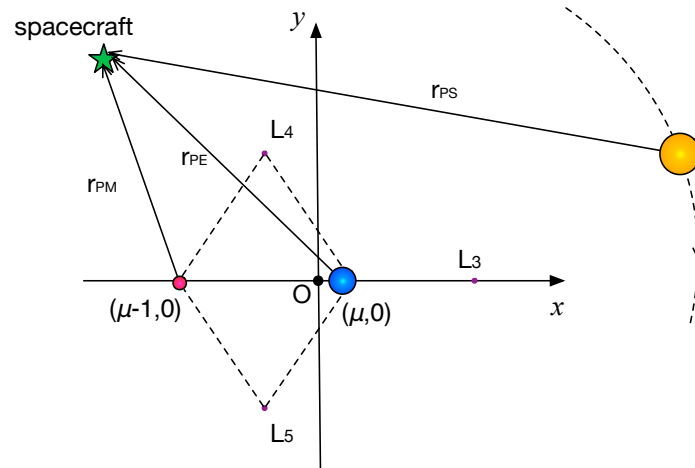
Fig. 1 BCP in the Earth-Moon rotating frame: the red, blue and yellow balls indicate the Moon, the Earth and the Sun, respectively.

2.2 Computation of Invariant Tori in BCP

In the CR3BP, the collinear libration points are unstable (of the form center × saddle) and, for the mass parameter of the Earth-Moon system, the triangular points are linearly stable. It is well-known that there exists Lyapunov families of periodic orbits emerging from the libration points in the center direction.

In the BCP, these libration points become periodic orbits with the same period as the perturbation, in this case, the period of the Sun $T_S = 2\pi/\omega_S$. More precisely, each of the collinear libration points is replaced by one unstable periodic orbit (of center × saddle type), and each of the triangular libration points is replaced by three periodic orbits, two stable and one unstable (center × saddle). Of these three periodic orbits, the unstable one is the closest to the triangular libration point [27].

Then, under generic non-resonance and non-degeneracy hypotheses, the effect of a periodic time-dependent perturbation on a periodic orbit family of an autonomous Hamiltonian is to produce a Cantorian family of quasi-periodic motions. Each of these quasi-periodic motions has two frequencies: the frequency of an unperturbed periodic orbit and the frequency of the periodic forcing [28]. In this situation, the Lyapunov families of periodic orbits of L_3 of the CR3BP become families of quasi-periodic motions. These quasi-periodic orbits are of saddle type, so each of them has stable and unstable invariant manifolds. Some of these stable manifolds intersect with the parking orbits around the Earth and some of the unstable manifolds go through the neighbourhood of L_4 providing a skeleton for the transfer.

The details about the computation of the family of Lyapunov invariant tori of L_3, their stability, invariant manifolds and discussions about the transport phenomena governed by L_3 in the BCP of the Earth-Moon-Sun system can be found in Ref. [35] and references therein. Actually, the initial conditions for the present work correspond to some results of Ref. [35]. For this reason, only a schematic version of the procedure for computation of tori and their manifolds is shown. The same process has been used to compute invariant tori around L_4, one of these tori is the final target orbit of the transfer.

For the computation of the two-dimensional torus, a temporal Poincaré map P_{T_s} corresponding to the period of the Sun T_S, is employed to obtain an autonomous four-dimensional discrete dynamical system. Each quasi-periodic motion becomes an invariant curve of the map P_{T_s}. The numerical methods used to compute these invariant curves and their stability are described in Ref. [38, 39]. Let us summarise them. Each invariant curve is represented in parametric from, $\varphi(\theta)$, $0 \leq \theta \leq 2\pi$, and must satisfy an invariance equation,

$$\varphi(\theta+\omega)=P_{Ts}(\varphi(\theta)) \tag{4}$$

where ω is the frequency of the invariant curve. For solving this equation, the invariant curve is expressed as a truncated Fourier series,

$$\varphi(\theta)=a_0+\sum a_k\cos(k\theta)+b_k\sin(k\theta) \quad (k=1, 2, \dots, N) \tag{5}$$

where N is the number of Fourier modes and a_0, a_k, and b_k are the Fourier coefficients. In order to find the specific set of Fourier coefficients and frequency for which the invariance equation holds, the invariant curve is discretized in $(2N+1)$ equally spaced points by evaluating Eq. (4) for angles $\theta_i = \frac{2\pi i}{2N+1}$, where $i=0, 1, \dots, 2N$ to obtain a non-linear set of equations for a_0, a_k, b_k, and ω, which are solved by means of a Newton method. The family is obtained by applying a standard continuation method using the arc parameter on the family as the continuation parameter.

The next step is to analyze the stability of each invariant curve by solving the following eigenvalue problem numerically

$$A(\theta)\psi(\theta)=\lambda\psi(\theta+\omega) \qquad (6)$$

where $A(\theta)=DP_{Ts}(\varphi(\theta))$ is the Jacobian of the Poincaré map on the curve $\varphi(\theta)$, and λ is the eigenvalue and $\psi(\theta)$ is the eigenfunction. The eigenfunction corresponding to a real hyperbolic eigenvalue gives the linear approximation to the associated invariant manifold [39]. This linear approximation is used to numerically produce the manifolds. The family of quasi-periodic orbits of L_3 is computed up to cover an 80% of the distance between L_3 and the Earth. They give rise to rich transport phenomena as discussed in Ref. [35]. This reference shows that the dynamical and geometrical aspects of the QPLOs of L_3 does not vary much along the family. Therefore, there is no big difference in the transport possibilities given by the invariant manifolds of different tori. Consequently, one medium-scale torus for the Lyapunov family of quasi-periodic orbits of L_3 is selected, in order to analyse all the possibilities that just one torus offers to construct the target transfers. An optimization of the transfers is a subject of further work.

To generate the invariant manifolds, a small displacement from the invariant curve along the stable and unstable directions is employed, from which the manifolds are produced by direct numerical integration either backward or forward in time. It is important to note that, near the invariant curve, by adjusting the magnitude of the displacement, the (x, y) projection of the stable and unstable manifolds overlap, which implies that there are (x, y) coordinates belonging to both manifolds (but with different velocities). These points allow for an easy transfer from the stable manifold to the unstable one. In the computations, 1000 points are taken along the selected invariant curve on the Poincaré section (that is, for $t=0$), as presented in Fig. 2. As shown in Fig. 2, the term invariant curve indicates the temporal section at $t=0$ of the selected medium-scale quasi-periodic Lyapunov orbit of L_3. The first two columns of the supplementary file list the x and y coordinates of these positions. The supplementary file is attached to this paper on the journal's webpage. They are arranged and denoted by #1-#1000 as shown in Fig. 2 and this notation will be used later.

Displace each of the 1000 points of the invariant curve along the stable and unstable directions and then propagate to compute a point on which the (x, y) coordinates belong to both the stable and unstable manifolds. To achieve this condition, the magnitude of the displacement has to be adjusted for each point and the final magnitude of the displacement is in the range of $[1.518\times10^{-7}, 1.764\times10^{-4}]$. Note that this process does not generate the full manifolds. To produce the complete manifolds, it is necessary to also consider a fundamental interval in the displacement direction to cover a fundamental cylinder of the manifold [35]. Although only a part of the manifolds is utilized, it is enough to obtain simple transfers from the stable to the unstable manifolds of the QPLO to produce trajectories going from the parking orbit around the Earth to the L_4 vicinity.
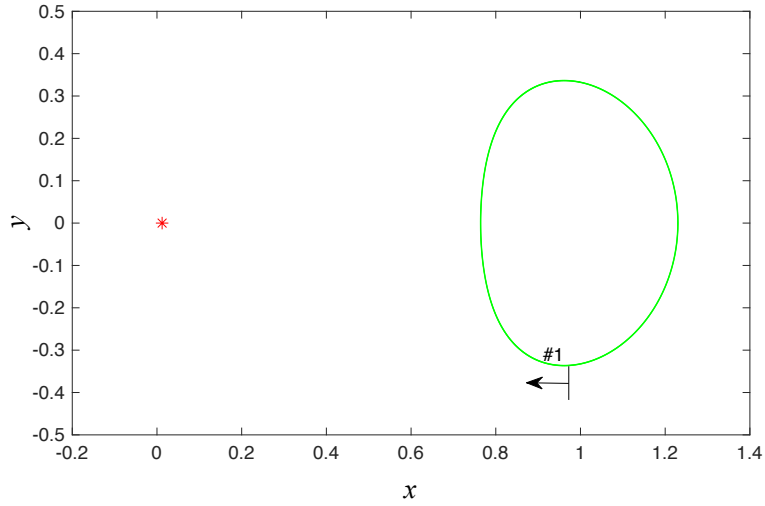
Fig. 2 Temporal section at *t*=0 of the selected medium-scale quasi-periodic Lyapunov orbit of L_3, projected in the (*x, y*) plane: the red star indicates the Earth.

2.3 Multiple Shooting Algorithm

To transfer the spacecraft from the stable to the unstable manifold of the QPLO a suitable maneuver is necessary to move away from a stable manifold trajectory, to pass at some distance of the QPLO and insert to another unstable manifold trajectory. Note that, to reduce the total TOF, it is important not to pass too close to the QPLO.

To this end and to obtain a smooth trajectory, a multiple shooting algorithm (see e.g., [40, 41]) is employed to fill the gap between the two patching segments, i.e., the stable manifold trajectory that the spacecraft departure and the corresponding unstable manifold trajectory that it inserts in this investigation. In the multiple shooting algorithm, a time interval [0, t_M] is divided into (*M*-1) subintervals [t_i, t_{i+1}], and $\Delta t = t_{i+1} - t_i$, *i*=1, 2, …, *M*-1. A state vector at a given time t_i can be given as

$$\mathbf{Q}_i = (x_i, y_i, \dot{x}_i, \dot{y}_i)^T, \ i = 1, 2, \ldots, M \tag{7}$$

The idea of the multiple shooting method is to integrate *M*-1 trajectories, one for each time subinterval, and to check if the final values of each trajectory coincide with the initial condition of the next, as shown in Fig. 3.

In this section, define χ($\mathbf{Q}_i$) as the mapping state vector of $\mathbf{Q}_i$ after a propagation time Δt. Then (*M*-1) continuity conditions must be satisfied as follows

$$F\begin{bmatrix} \mathbf{Q}_1 \\ \mathbf{Q}_2 \\ \vdots \\ \mathbf{Q}_{M-1} \end{bmatrix} = \begin{bmatrix} \chi(\mathbf{Q}_1) \\ \chi(\mathbf{Q}_2) \\ \vdots \\ \chi(\mathbf{Q}_{M-1}) \end{bmatrix} - \begin{bmatrix} \mathbf{Q}_2 \\ \mathbf{Q}_3 \\ \vdots \\ \mathbf{Q}_M \end{bmatrix} = 0 \tag{8}$$

where $\boldsymbol{F}$ denotes the deviation between χ($\mathbf{Q}_i$) and $\mathbf{Q}_{i+1}$. Hence, a system of 4(*M*-1) equations is built up with 4*M* variables given the planar BCP. In this investigation, the position coordinates of both the initial and final points are fixed to guarantee the successful matching between two trajectories but the velocity coordinates are regarded as variables. The constraint on the position coordinate of the first and last points can be expressed as

$$\begin{cases} \mathbf{Q}_1 = [x_{initial}, y_{initial}, *, *] \\ \mathbf{Q}_M = [x_{final}, y_{final}, *, *] \end{cases} \tag{9}$$

where ($x_{initial}$, $y_{initial}$) and (x_{final}, y_{final}) denote the position coordinates of the fixed initial and final points on the two trajectories to be patched. The velocity coordinates are indicated by * which are not fixed. Thus, 4(M-1) equations with 4(M-1) variables are solved in each iteration of the algorithm. Then a unique solution to Eq. (8) is obtained through an iterative numerical algorithm based on the classical Newton's method.
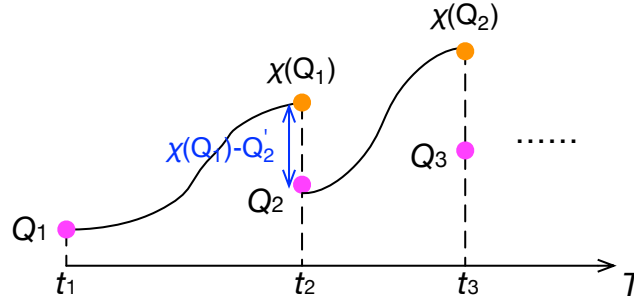

Fig. 3 A schematic plot of the multiple shooting method.

3. Transfer via Stable/Unstable Manifolds of L_3 Lyapunov Orbits

3.1 Unstable Manifolds to L_4 Vicinity

As aforementioned, the BCP model exhibits three periodic orbits (with the period of the Sun) around L_4. The closest one to L_4 is denoted as OP1 in Ref. [29, 38], and its linear stability is of saddle × center type. The instability of the saddle is very mild. The quasi-periodic orbits family corresponding to the center direction up to some distance from OP1 is produced, as illustrated in Fig 4. The inner part in the (x, y) plane is filled by invariant curves (except by a set of very small gaps corresponding to resonances, too small to be relevant [28]). The spacecraft is finally inserted to one of these invariant curves, i.e., quasi-periodic orbits, that intersects with an unstable manifold trajectory of the QPLO of L_3 at their common epoch, after performing an injection maneuver.

A necessary condition for a successful insertion is that the end of such transfer trajectories locates on or inside these curves. The union of these curves indicates the largest boundary containing all possible insertion points. The target invariant curve, i.e., the quasi-periodic orbit around L_4 is computed at epoch t that satisfies $\mathrm{mod}(t,T_S)=t_0$, where $T_S=2\pi/\omega_S$ denotes the synodic period of the solar gravity in the Earth-Moon rotating frame and t_0 indicates a specific epoch. Ten specific epochs are taken, i.e., t_0=0, $0.1T_S$, $0.2T_S$…, $0.9T_S$, respectively, corresponding to $t=KT_S$, $(0.1+K)T_S$, $(0.2+K)T_S$…, $(0.9+K)T_S$, where K indicates arbitrary non-negative integer. Fig. 4 illustrates the (x, y) projection of this outermost invariant curve around L_4 at these ten epochs, i.e., t_0=0, $0.1T_S$, $0.2T_S$…, $0.9T_S$, respectively. The green "cloud"-shaped line in Fig. 5 indicates the union of the (x, y) projections of the outermost invariant curve at t_0=0, $0.1T_S$, $0.2T_S$…, $0.9T_S$. The performance of the unstable manifolds of the selected QPLO of L_3 to the vicinity of L_4 is presented on a special Poincaré section $\{\Sigma_\beta: \arctan(y/(x-\mu))=\beta\}$, as shown in Fig. 5. A sequence of this Poincaré sections is used varying the value of β equally distributed between the lower and upper boundary, i.e., 1.6937 rad, 1.7810 rad, 1.8683 rad, 1.9556 rad, 2.0429 rad, 2.1302 rad, 2.2175 rad, 2.3048 rad, 2.3921 rad, respectively, cutting transversally the green "cloud" as shown in Fig. 5. The green "cloud"-shaped line intersects with Σ_β twice for each β and r_{min} and r_{max} indicates distance from the Earth to the closer and farther intersection points. As declared in **Section 2.2**, all the unstable/stable manifolds generated from the selected QPLO

around L_3 are indexed from 1 to 1000 and referred by their index[1]. To detect how these unstable manifold trajectories approach to the L_4 vicinity, their intersections with Σ_β are obtained and shown in Fig. 6, where r indicates the distance from the intersection points between the unstable manifold trajectories to the Earth. The TOF of the unstable manifold trajectories from the L_3 vicinity to the L_4 vicinity is denoted as $\text{TOF}_{unstable}$ and the TOF of the stable manifold trajectories from the Earth vicinity to the L_3 vicinity is denoted as TOF_{stable}.

The plot of the unstable manifolds of the QPLO around L_3 with $r \in [r_{min}, r_{max}]$ at a specific value of β suggests that they pass in position through the invariant curves of L_4 and an insertion to a quasi-periodic orbit around L_4 is feasible. It is important to notice that only the first passage of the manifolds near L_4 is considered. Further passages may provide better transfers but with a longer TOF. Through the examination on $r \in [r_{min}, r_{max}]$, some members of the unstable manifolds are not considered and the remaining ones are presented in Fig. 6. The horizontal axis indicates the index of the initial state of the unstable manifold trajectories from 1 to 1000 and vertical axis indicates the value of β of Σ_β that intersects with the unstable manifold trajectory satisfying $r \in [r_{min}, r_{max}]$. The tint of colour in Fig. 6(a) and 6(b) indicates the value of r, and the corresponding TOF, respectively. Wherein a large blank area exists in the middle, suggesting that trajectories inside the unstable manifold starting at points #450-#610 lead to no connections to L_4. Note that to unify the description, "the trajectories inside the stable (or unstable) manifold starting at points #X, e.g., #5" is mentioned as "#5 stable manifolds trajectory" or "stable manifolds trajectory of initial condition #5" in the following sections. A single trajectory on the unstable manifold can intersect several Poincaré sections Σ_β for different phase angle β, e.g., trajectories #1-#76 go through the Poincaré sections Σ_β for $\beta=1.9556$ rad and 2.0429 rad. According to the data uploaded in the supplementary document and also the Fig. 2, #1-#76 and #900-#1000 unstable manifolds trajectories are generated from the bottom part of the quasi-periodic Lyapunov orbit with negative y coordinate. More intersections with Poincaré sections Σ_β lead to more insertion chances. According to Fig. 6(b), the total range of TOF of segments from the L_3 vicinity to the L_4 vicinity is 55-69 days, which is an acceptable value so far. As shown in Fig. 6, the feasible unstable manifolds generate from the initial condition set

$$U_1=\{\#1\text{-}\#76, \#82\text{-}\#105, \#148\text{-}\#156, \#168\text{-}\#270, \#292\text{-}\#317, \#336\text{-}\#416, \#437\text{-}\#443,$$
$$\#614\text{-}\#683, \#701\text{-}\#749, \#774\text{-}\#796, \#802\text{-}\#807, \#835\text{-}\#841, \#848\text{-}\#872, \#878\text{-}\#1000\},$$

in the selected quasi-periodic Lyapunov orbit of L_3.

By such preliminary examination, the unstable manifolds connecting the L_3 vicinity to the L_4 vicinity are selected geometrically. Later, the final time in the unstable manifold trajectory must be confirmed to match the insertion time into the quasi-periodic orbits around L_4. The purpose of such two-step implementation on the unstable manifolds is to provide a regularized process to conduct this construction method and release the burden of manual work the results as much as possible. The outermost curve around L_4 at each epoch is irregular and can not be mathematically expressed. Thus, whether the unstable manifolds trajectories pass through the inner part of the curve must be checked one by one by manual work if the geometric information of the unstable manifolds trajectories is mixed up with their time information. In other words, at least 1000×10 insertion points along 1000 unstable manifolds trajectories have to be checked whether they are inside or on the outermost invariant curve around L_4 at ten epochs. However, through the preliminary examination on geometric information, those unstable manifolds that

---

never intersect with any quasi-periodic orbit around L_4 are not considered. After another selection in next section on the perigee altitude of their corresponding stable manifold trajectories, the set of the feasible unstable manifold trajectories is further narrowed. Then it becomes easier to finally check the time information of the intersection points of the remaining unstable manifolds.


(a)

(b)

(c)

(d)

(e)

(f)
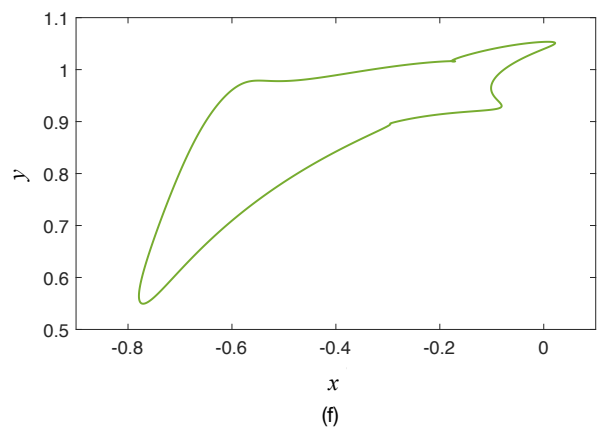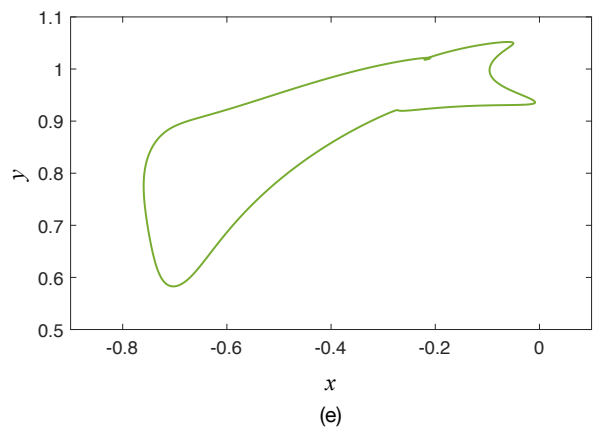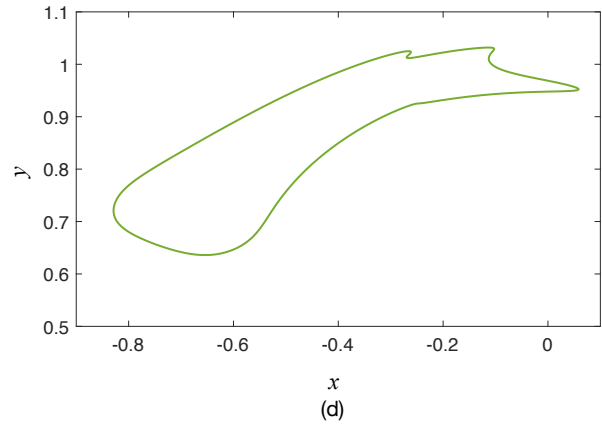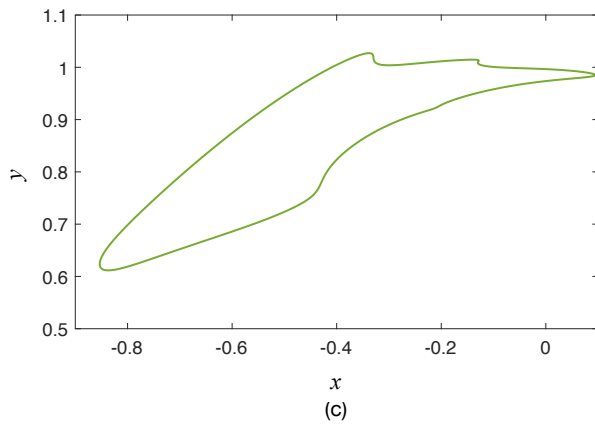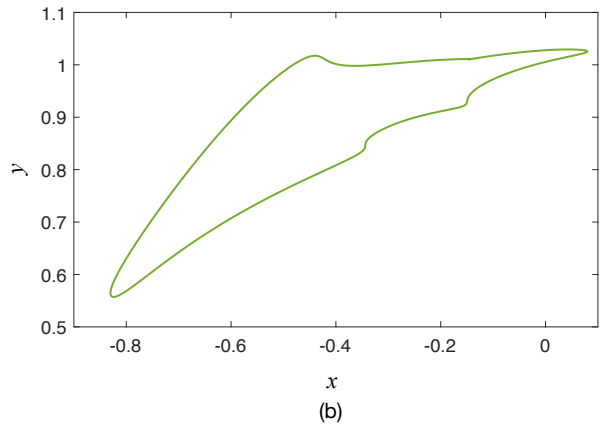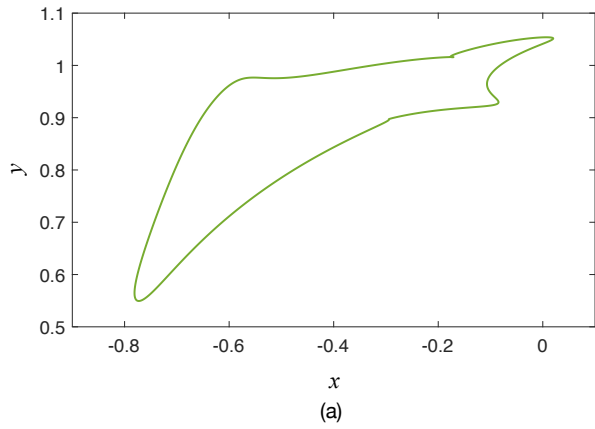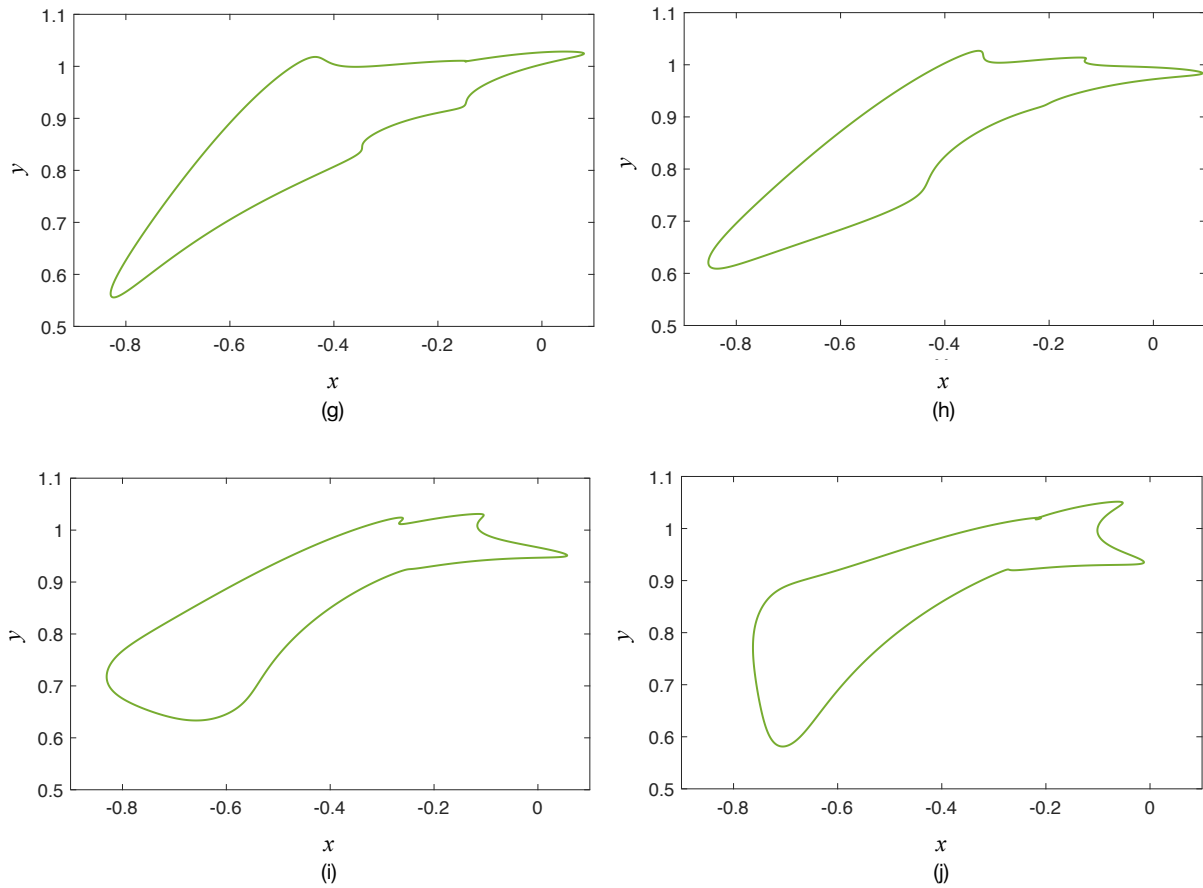
Fig. 4 The outermost computed curve of the corresponding center manifolds of L_4 at different t_0: 0(a), 0.1T_S(b), 0.2T_S(c), 0.3T_S(d), 0.4T_S(e), 0.5T_S(f), 0.6T_S(g), 0.7T_S(h), 0.8T_S(i), and 0.9T_S(j).
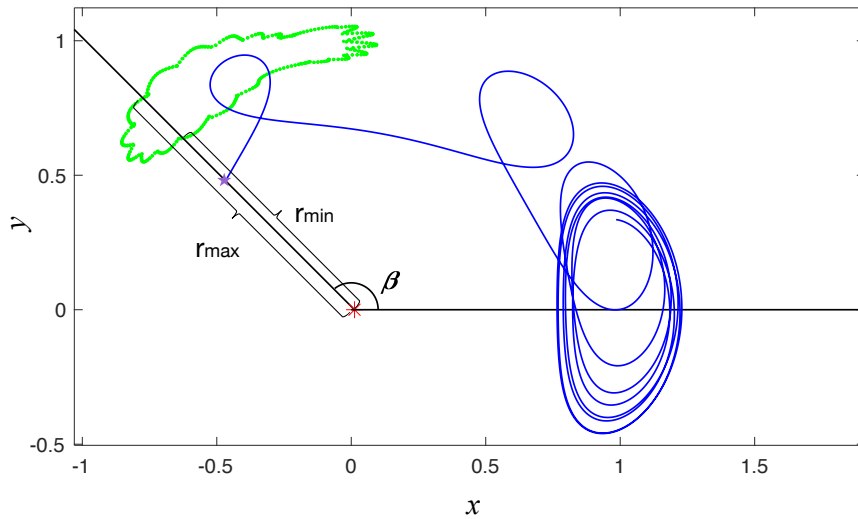
Fig. 5 Poincaré section Σ_1 (black) and an example unstable manifold trajectory of the selected quasi-periodic Lyapunov orbit around L_3 (blue): the purple star indicates the intersection point; the red mark indicates the Earth.
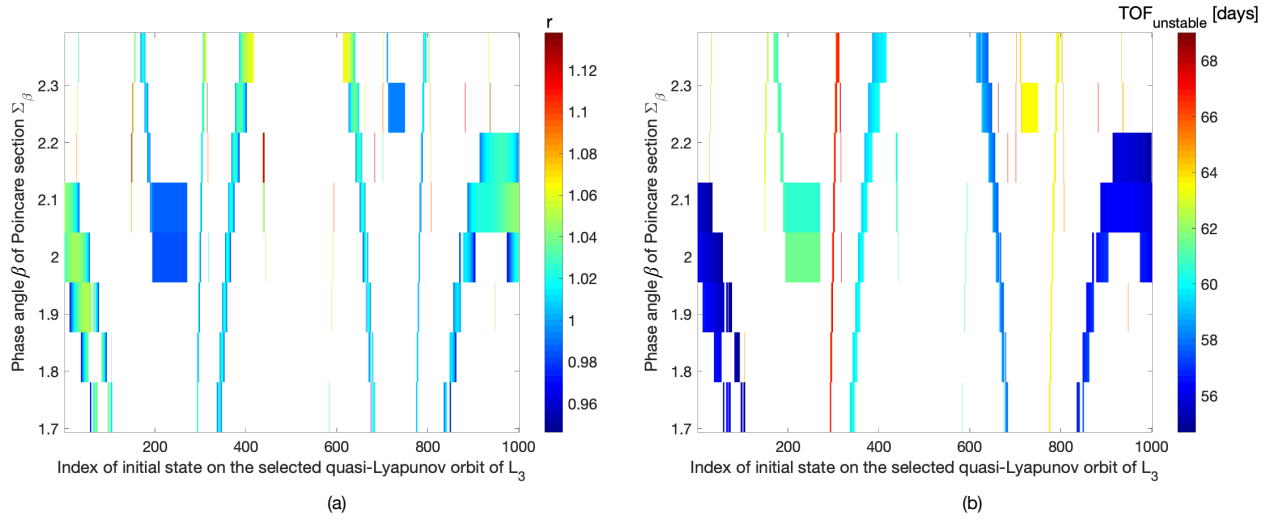
Fig. 6 The value of r (a) and TOF$_{unstable}$ (b) of the feasible unstable manifolds.

3.2 Stable Manifolds to Earth Parking Orbits

The trajectories starting at (x, y) coordinates in U_1 (presented in **Section 3.1**) with the corresponding velocities in order to be on the stable manifold are used to construct transfer segments connecting the L_3 vicinity and the circular Earth parking orbits. Initially, the same location near the quasi-periodic Lyapunov orbit around L_3 is used for arrival of the stable and departure of the unstable manifolds. This constraint is later removed as a multiple shooting algorithm is introduced.

Instead of fixing the altitude of the parking orbit, a range of potential parking orbits are considered from the altitude of geostationary orbits (about 0.12 in dimensionless unit) to the altitude of low parking orbits (about 0.017 in dimensionless unit). Within the propagation time of 40 months backward in time, the stable manifolds without perigee distance in this range are regarded improper to construct the Earth transfer segments and abandoned. Then, a spacecraft is inserted from a circular Earth parking orbit to the selected stable manifold segment by means of an orbital maneuver implemented at the perigee of the stable manifold segment. The fuel consumption and the TOF$_{stable}$ is related to the altitude of the Earth parking orbits.

As shown in Fig. 7, the initial condition set of feasible trajectories on the stable manifold is furtherly narrowed by the previous selection strategy based on U_1. In particular, the feasible trajectories generate from the initial condition set

$U_2=\{$#11, #21, #37, #38, #47, #58, #65, #151, #178, #190, #316, #337, #349, #372, #373, #631, #633, #646, #649, #660, #662, #670, #710, #777, #784, #787, #793, #851, #853, #862, #865, #872, #878, #889, #895, #896, #900, #908-#917, #937, #938, #966, #970, #971, #975-#984, #993, #997$\}$,

in the stable manifold of the selected quasi-periodic Lyapunov orbit of L_3. They all have maneuver chances at several perigees, e.g., #914 stable manifold segment approaches the Earth at 78 different perigees with their perigee distance ranging from 0.02 to 0.11 and fuel consumption varying from 2.85 km/s to 1.0 km/s. A trajectory can only have one perigee, which is its closest approach to the center body. In this investigation, the term "perigee" is extended to those points that has a local minimum distance with respect to the center body, along a multiple close trajectory. Fig. 7(a) shows that the fuel consumption for maneuver highly depends on the altitude of the parking orbit and

varies from 1.0 km/s to 2.85 km/s. Obviously, they follow the rule that the higher the altitude of the Earth parking orbit, the less the fuel consumption.

The distribution of the parameter TOF$_{stable}$ is illustrated in Fig. 7(b) and it varies from 300 days to over 1000 days. The TOF$_{stable}$ to approach L_3 is dominant over the total transfer time. The distribution of TOF$_{stable}$ does not follow the similar rule as the fuel consumption. As shown in Fig. 7(b), perigees in the four black boxes lead to quicker transit (shorter than 550 days) from lower circular Earth parking orbits (with altitude less than 0.04) to the L_3 vicinity by the related stable manifolds trajectories. Thus, the transfer segments from the Earth to the L_3 vicinity are picked out by carefully combining the fuel consumption, the TOF$_{stable}$ and the perigee distance based on various engineering requirements.
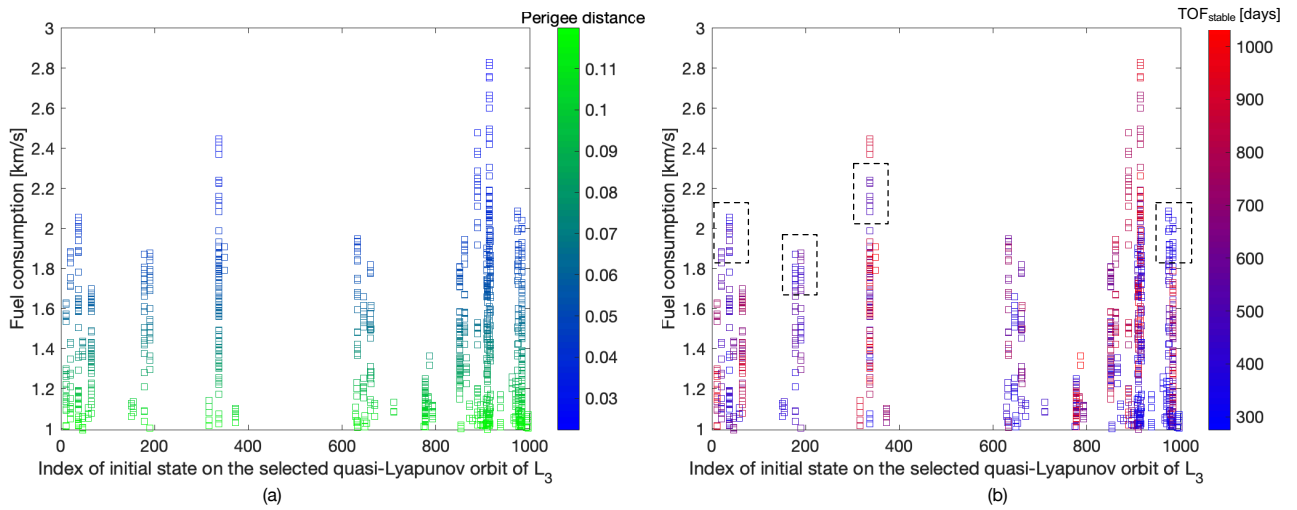

Fig. 7 The distribution of perigee distance (a) and TOF$_{stable}$ (b) of feasible stable manifolds generated from set U_2.

3.3 Insertion Point Selection

In **Section 3.1**, a preliminary selection based on the geometrical necessary condition is completed to pick out feasible trajectories passing through the neighborhood of L_4. In this step, the time necessary condition is examined for the survival unstable manifold trajectories. For this purpose, the Poincaré section $\{\Sigma_t: \mathrm{mod}(t,T_S)=t_0\}$ is implemented to slice the unstable manifold trajectories generated from the initial condition set U_2 (presented in **Section 3.2**) at different $t_0=0, 0.1T_S, \ldots, 0.9T_S$. The projection of the unstable manifold trajectories chosen in **Section 3.2** onto the (x, y) plane and the corresponding invariant curve at $t_0=0, 0.1T_S, \ldots, 0.9T_S$ are presented in Figs. 8(a), 8(b), …, 8(j), respectively. The trajectories starting at U_2 following unstable direction arrive at the specific location marked as blue diamonds at a specific time. Thus, all of the blue diamonds inside or on the boundary of the invariant curve indicate feasible insertion points, where the spacecraft is inserted in a quasi-periodic orbit around L_4 by means of an orbital maneuver. According to Fig. 8, the insertion chances are not equal at each moment t_0 and more insertion opportunities arise during the half period from $0.1T_S$ to $0.6T_S$. A careful check on the results shows that at the same t_0, there can be several insertion points along a single unstable manifold trajectory. A single unstable manifold trajectory from U_2 does not need to lay exactly on the invariant curve at all epochs $t_0=0$, $0.1T_S, \ldots, 0.9T_S$, but each unstable manifold trajectory from U_2 must goes through the invariant at at least one epoch t.

Initial conditions from the set U_2 generate both stable and unstable manifolds segments connecting the Earth and the L_4 vicinity, respectively. **Section 2.2** discussed the existence of couples of trajectories (one inside the stable manifolds, one inside the unstable manifolds) sharing a point with the same (x, y) coordinates. At these points, a velocity change generally smaller than 1.5×10^{-5} m/s m/s is requested to switch a spacecraft from the stable manifold to the unstable one. Fig. 9 presents four sample feasible transfer trajectories by the stable and unstable manifolds trajectories of initial condition #37, #646, #853, and #938.

Furthermore, the fuel consumption at each insertion point is presented in Fig. 10. The minimum and maximum value at each epoch is listed in Table 2. As illustrated in Fig. 10, 213 insertion points are obtained in this investigation at 10 specific moments serving as insertion points to the neighborhood of L_4. The general fuel consumption at them is smaller than 310 m/s. Compared with the results in **Section 3.2**, they are far smaller than the value at perigee points of the circular Earth parking orbits. To further reduce the total fuel consumption, an optimization algorithm is supposed to be applied targeting at the near-Earth segments. However, the optimal fuel consumption is not the goal of this investigation, so they are not discussed in this paper.

So far, a new approach using stable and unstable manifolds of a QPLO around L_3 to construct transfer segments connecting the Earth parking orbits and the L_4 vicinity is validated. The stable and unstable manifolds used are generated from the same initial condition along the QPLO so that a switch from the stable manifold trajectory to the unstable one is smooth in the sense of time and position. In the next section, the stable and unstable manifolds from different initial condition are combined together by a multiple shooting method in order to control the loops around L_3.

**Table 2 The minimum and maximum fuel consumption at the final insertion near L_4**

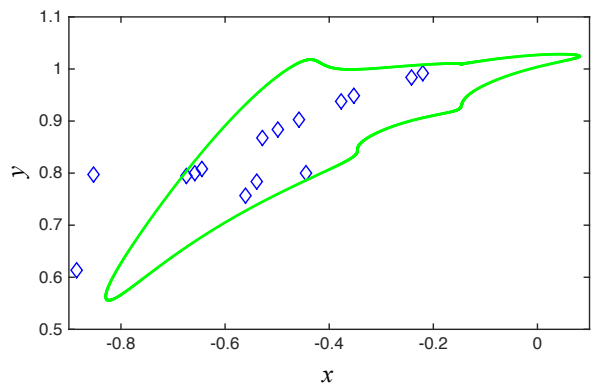| Insertion epoch	Minimum Δv at insertion points	Maximum Δv at insertion points
$t_0=0$	102.48 m/s	296.42 m/s
$t_0=0.1T_S$	153.31 m/s	301.72 m/s
$t_0=0.2T_S$	129.75 m/s	190.74 m/s
$t_0=0.3T_S$	94.82 m/s	188.57 m/s
$t_0=0.4T_S$	77.91 m/s	288.51 m/s
$t_0=0.5T_S$	132.34 m/s	271.77 m/s
$t_0=0.6T_S$	117.86 m/s	271.10 m/s
$t_0=0.7T_S$	144.82 m/s	200.47 m/s
$t_0=0.8T_S$	118.27 m/s	140.54 m/s
$t_0=0.9T_S$	132.54 m/s	223.29 m/s

(a)

(b)

(c)

(d)

(e)

(f)

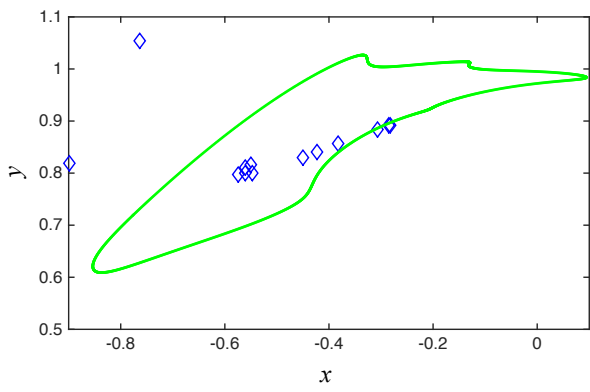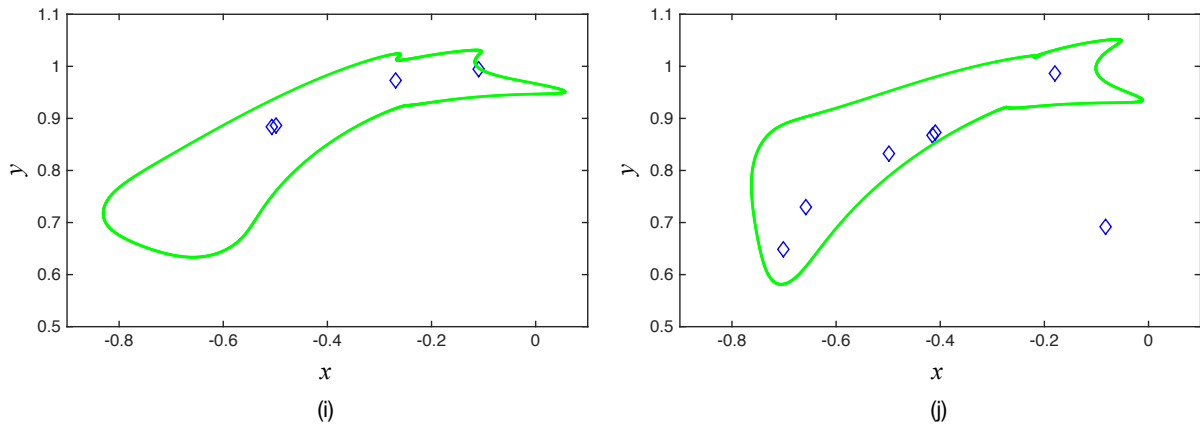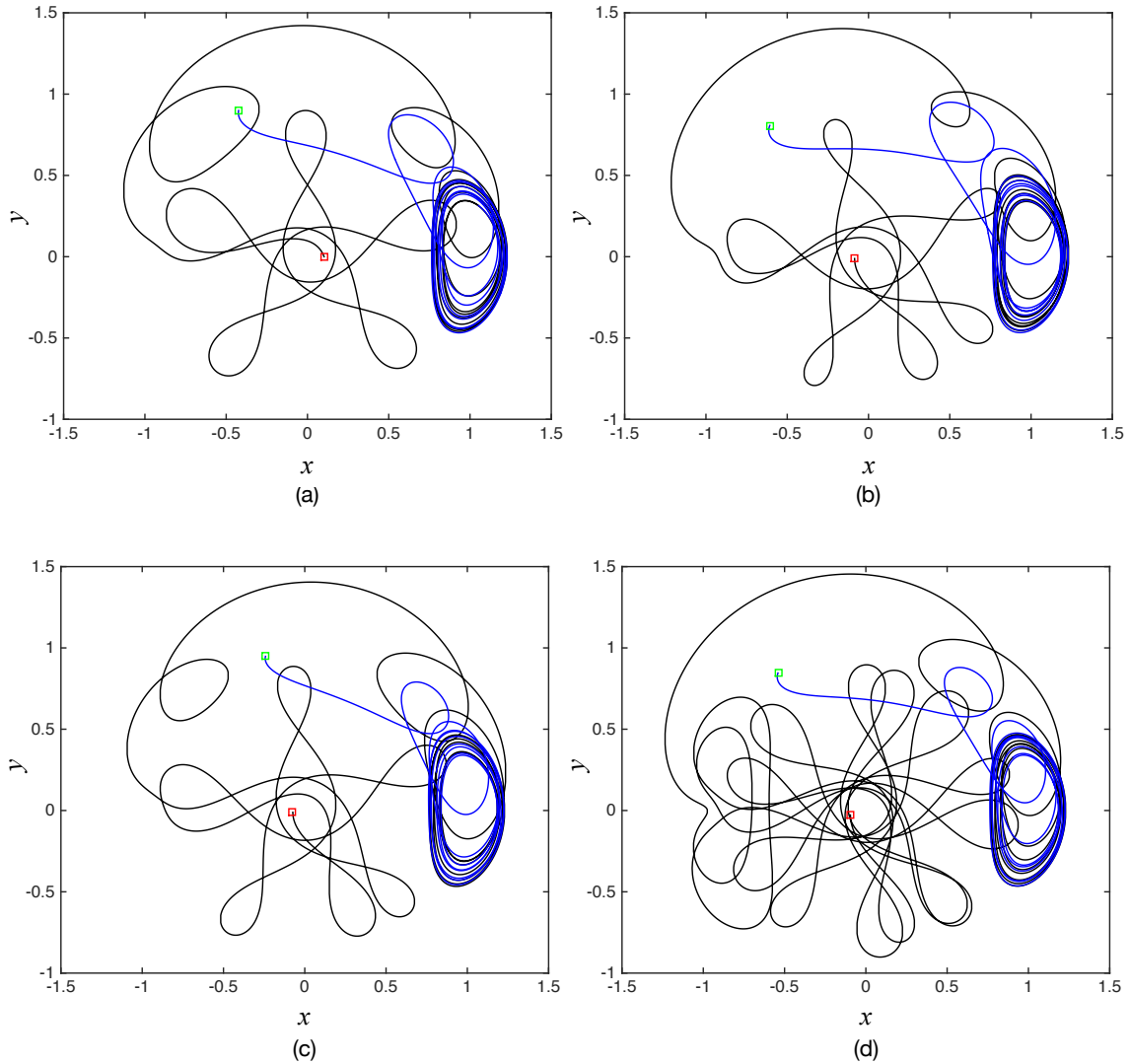(g)

(h)

(i)   (j)
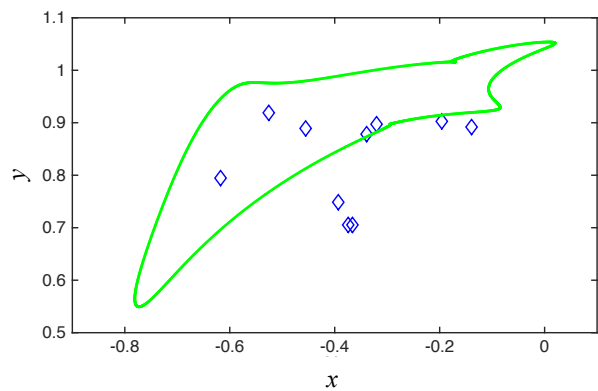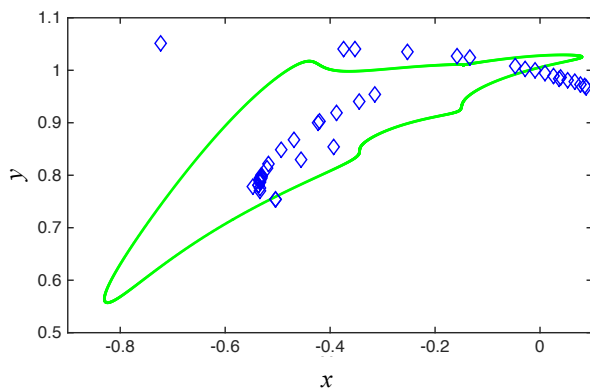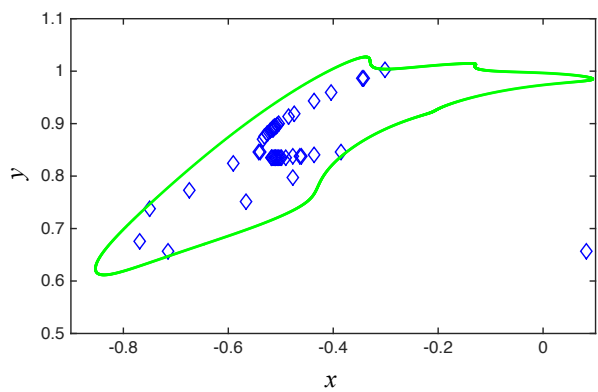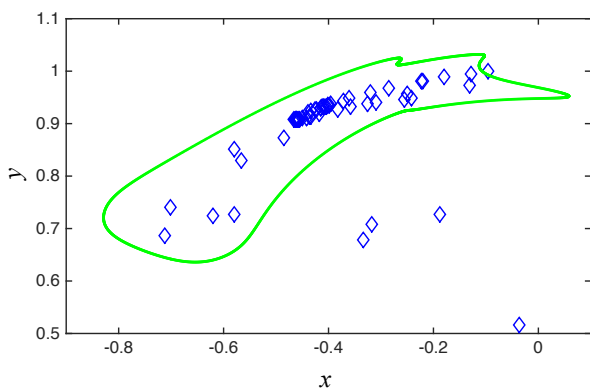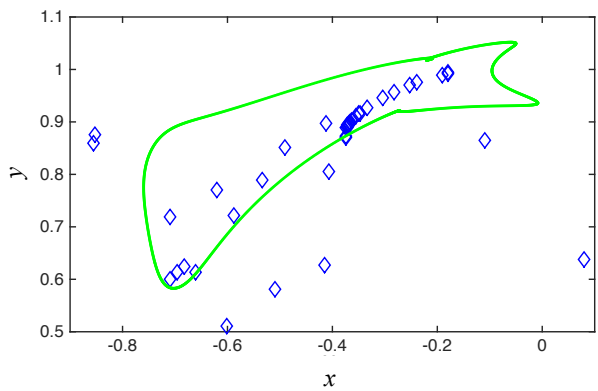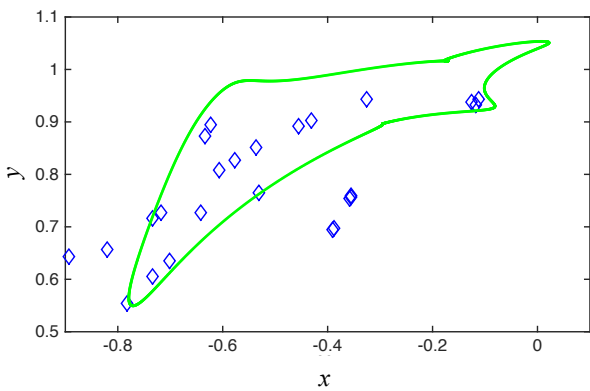
Fig. 8 The projection of the unstable manifolds chosen in Section 3.1 onto (x, y) plane (blue diamonds) and the most outer curve of stable regions around L_4 (green curves) at t_0=0(a), $0.1T_S$(b), $0.2T_S$(c), $0.3T_S$(d), $0.4T_S$(e), $0.5T_S$(f), $0.6T_S$(g), $0.7T_S$(h), $0.8T_S$(i), and $0.9T_S$(j).

(a)   (b)

(c)   (d)

Fig. 9 Four examples of feasible transfer trajectories using stable (black) and unstable (blue) manifolds trajectories of initial condition #37, #646, #853, and #938: red squares indicate the first perigee with perigee distance smaller than 0.10; green squares indicate the insertion points near L_4.
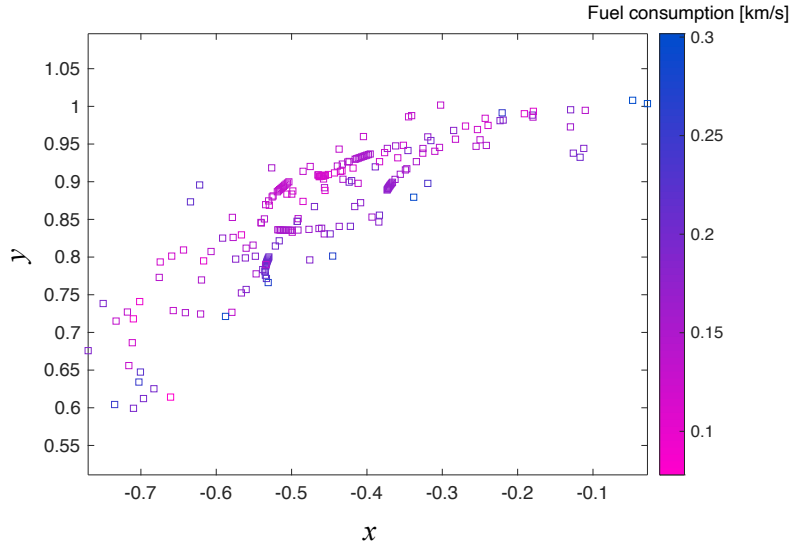
Fig. 10 Fuel consumption at all insertion points near L_4.

4. Multi-revolution Behavior around L_3

4.1 Combining Different Stable and Unstable Manifolds

The escaping rate of trajectories along stable/unstable directions can be qualified by the stability index (calculated from the eigenvalues related to hyperbolic motion). In the CR3BP, the stability index related to hyperbolic motion of Lyapunov orbits of L_1 and L_2 have normally a magnitude of over 10^4, remarkably larger than the value of Lyapunov orbits of L_3 [42]. This value does not alter very much even with solar gravity perturbation added. Instead, the solar gravity promotes the unfolding and divergence of stable/unstable manifolds of QPLOs in the sense that they go towards various targets such as the Earth, Moon and L_4 [35]. However, note that trajectories passing near an invariant object (fixed point, periodic or quasi-periodic orbit, etc) stay close to it for a long time. A trajectory along the stable manifolds towards the QPLO conducts a long-term looping towards around L_3, so that the total TOF highly depends on the time spent near L_3.

A quick way to reduce the time spent near the QPLO is to patch the arrival segment to another departure segment at some distance of the QPLO, to avoid spending a lot of time looping around the QPLO. In other words, the initial constraint on the same (x, y) location used for arrival of the stable and departure of the unstable manifolds is removed in this section. This patching technique is successfully used in the literature to construct homoclinic/heteroclinic connections [43] or low-energy transfers [44] via stable and unstable manifolds. In these works, the patching is implemented in an autonomous phase space. Here, the matching of stable and unstable segments is carried out in two dimensions plus the time.

The basic goal is to build up a "shortcut" trajectory by managing the multi-revolution behaviour of the unstable and stable manifolds. For this purpose, a Poincaré section $\{\Sigma_2 : y=0\}$ is used to record intersection points of trajectories inside stable and unstable manifolds from the initial condition set U_2. To increase the patching opportunity, the sign of $\dot{x}$ for the intersection points in this step is not specified. Fig. 11 illustrates their projection onto (x, t) plane, where the intersection points of stable and unstable manifolds generated from the same initial condition are plotted by the same color. The star indicates the intersection points of the stable manifolds and Σ_2

while the dot indicates those of the unstable manifolds. Most of the intersection points look like two smooth curves, with their x coordinates in the range of [0.75, 0.85] and [1.15, 1.25], corresponding to both positive and negative $\dot{x}$, respectively. Fig. 11(b) demonstrates that on each curve, there exist intersection points of stable manifolds close enough to some of the unstable manifolds. An examination on the data of Fig. 11(a) shows that the minimum distance between any two intersection points is 5.736×10^{-5}, which is small enough to implement any patching method. The intersection points with distance smaller than 1×10^{-3} are searched for, as shown in Fig. 12. A diamond mark in Fig. 12 indicates one intersection pair that contains one intersection point of a stable manifold trajectory and another one of an unstable manifold trajectory. The stable and unstable manifolds are not generated from the same initial condition along the QPLO around L_3. The horizontal axis indicates how many times both the stable and unstable manifolds segments cross Σ_2 before the corresponding intersection point pair. Note that the total number of intersections with Σ_2 at one intersection point pair is about twice of the number of the loops that the corresponding stable and unstable manifolds segments conduct. The larger the value is, the more loops the stable and unstable segment pairs achieve before the corresponding intersection point pair, and the more loops will be replaced through patching.

One of the general ways to connect (in phase space) two intersection points in Fig. 11(a) is the shooting method. In this investigation, a multiple shooting algorithm is developed to patch the stable and unstable manifold segments indicated by the intersection pairs in Fig. 12. In the implementation of the multiple shooting algorithm, the position coordinates of both the initial and final points are fixed along the corresponding stable and unstable manifolds segments. The idea of the multiple shooting algorithm in this investigation is to fully remove the discontinuities in x coordinate (in the Σ_2 section $y=0$) guaranteeing the same epoch t, in order to get a smooth transition from the stable to the unstable manifold segments.

Taking #2 patching pair in Fig. 12 to describe how to locate the starting points for patching along the stable manifold segments and the final points along the unstable manifold segments. Suppose the associated stable manifold trajectory intersects with Σ_2 at epoch t and the associated unstable one intersects with Σ_2 later at $(t+\mathrm{d}t)$. First implement numerical integration backwards in time along this unstable manifold trajectory from its intersection point to obtain its state (or position) at t. Thus, the positions that the stable and unstable manifold trajectory arrives at the same epoch t are obtained. Denote the position vectors on the stable and unstable manifold trajectory as X_{stable}^{t} and $X_{unstable}^{t}$, respectively. Then, choose the time length Δt for the patching arc. The value of Δt is experimentally set as $\pi/10$ in this investigation. It is not fixed but can be chosen flexibly according to the problem itself. Next, find the position that the stable manifold trajectory approaches at the epoch $(t-\Delta t/2)$ and the position that the unstable manifold trajectory arrives at the epoch $(t+\Delta t/2)$. Denote these position vectors on the stable and unstable manifold trajectory as $X_{stable}^{t-\Delta t/2}$ and $X_{unstable}^{t+\Delta t/2}$, respectively. They indicate the starting and the final points of a patching arc and the segments from $X_{stable}^{t-\Delta t/2}$ to X_{stable}^{t} and the one from $X_{unstable}^{t}$ to $X_{unstable}^{t+\Delta t/2}$ constitute the patching arc to be dealt with by the multiple shooting algorithm. Finally, the multiple shooting algorithm is implemented, as shown in **Section 2.3**. Note that the velocities along x and y axis at the starting and final points of the patching arc are regarded as variables in the multiple shooting algorithm and adjusted by impulsive thrust. The tolerance to solve $\boldsymbol{F}=\boldsymbol{0}$ in Eq. (8) is set to 10^{-10}, which is satisfied after 3-4 iterations of the Newton method. As a powerful tool, the multiple shooting method works well once the initial guess is close enough to the solution, e.g., their distance is smaller than 1×10^{-3}

in this investigation.

(a)   (b)
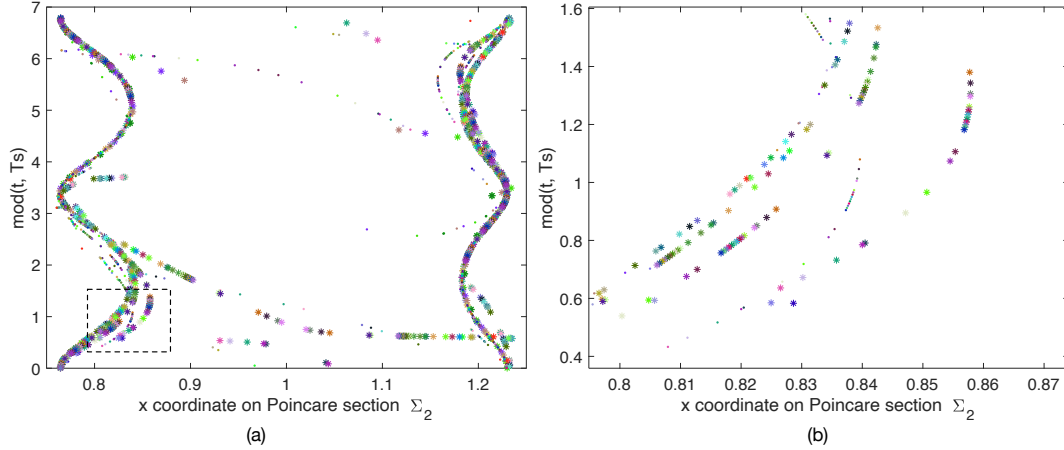
Fig. 11 The projection of intersection points with Poincaré section Σ_2 onto (x, t) plane (a) and a zoom-in region (b).
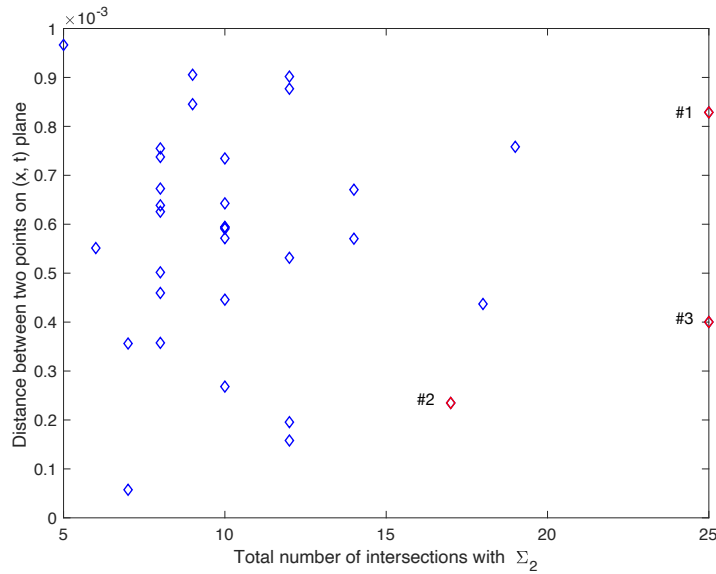
Fig. 12 The intersection points with distance smaller than 1×10^{-3}.

4.2 Patching Trajectories by Multiple Shooting Method

As explained in **Section 3.2**, the transfer segments from the Earth to the L_3 vicinity are determined by the perigee points selected and thereby the corresponding TOF as well as fuel consumption. The spacecraft stays a long time looping around the Earth before escaping from the Earth vicinity. Thus, instead of presenting the whole stable manifolds, the first perigee with distance of 0.1-0.1093 (the altitude of geostationary satellites, about 35600 km) is chosen as the insertion point from the circular Earth parking orbit to the stable manifolds.

The information displayed in Fig. 12 does not only contribute to the reduction of loops around L_3 (and thereby to reduce the total TOF), but also provides us information on how to design multi-loop trajectories around L_3 by patching the intersection points. Through a chosen number of loops, a specific looping time around L_3 is achieved in order to satisfy the mission requirements. For example, for a quick transit via L_3 QPLOs to L_4 vicinity, a patched trajectory is chosen with as few loops around L_3, as presented in Fig. 13(b). The trajectory shown in Fig. 14(b) has only 10 loops around L_3 for over 100 days with 9 loops eliminated through patching, and a spacecraft can visit both

L_3 and L_4 in a single transfer with a low fuel consumption of 75 m/s. In this section, three pairs of patching points with different loops are chosen from Fig. 14 to show the refined results by the multiple shooting method, as indicated by the red diamonds in Fig. 12.

The selected patching pairs are $(25, 0.825\times10^{-3})$, $(17, 0.23\times10^{-3})$ and $(25, 0.410^{-3})$, numbered as #1, #2, and #3 patching pair in Fig. 12, and their matching results are shown Figs. 13 and 14, respectively. The first patching pair belongs to the #337 stable manifolds trajectory and to the #349 unstable manifolds trajectory and the corresponding intersection point of the #349 unstable manifolds trajectory is indicated by the right red square in Fig. 13(a). The left red square indicates the perigee point from a circular Earth parking orbit to the stable manifolds. As shown in Fig. 13(a), along the #349 unstable manifolds trajectory, there are three insertion points to a quasi-periodic orbit around L_4 at $t_0=0.7T_S$, $0.8T_S$ and $0.9T_S$, indicated by the green squares. Two small segments are selected along #337 stable and #349 unstable manifolds trajectory from the patching pair to implement the multiple shooting method. The refined trajectory is indicated by the red line in Fig. 13(c). Since the distance between two points on (x, t) plane of the first patching pair is smaller than 1×10^{-3} as illustrated in Fig. 12, the fuel consumption requested at the boundary points of this refined trajectory is very small, i.e., 33.0335 m/s and 36.4655 m/s, respectively. The TOF for the unstable manifold segment ending at the insertion point around L_4 at $t_0=0.9T_S$ is 9.4912 days and the TOF for the stable manifold segment and the patching segment in total is 166.49 days. The corresponding fuel consumption is 150.00 m/s and 1494.85 m/s, respectively. Comparing Fig. 13(a) and 13(b), it is seen that through matching the first pair by multiple shooting method, about 12 loops are suppressed and 225.54 days are saved correspondingly. The remaining loops around L_3 take about 54.67 days. Thus, through the first patching pair, most of TOF around L_3 is eliminated so that a quicker transfer is achieved based on #337 stable and #349 unstable manifold trajectories.

The situation corresponding to the second patching pair is different as shown in Figs. 14(a) and 14(b), where more loops remain. The second patching pair belongs to #774 stable manifold trajectory and #178 unstable manifold trajectory and the intersection point of the #178 unstable manifold trajectory is indicated by the right red square in Fig. 14(a). The left red square indicates the perigee point from the circular Earth parking orbit to the stable manifolds. Along #178 unstable manifold trajectory, there are three insertion points to a quasi-periodic orbit around L_4 at $t_0=0$, $0.1T_S$ and $0.9T_S$, indicated by the green squares in Figs. 14(a) and 14(b). Small segments are selected along #774 stable and #178 unstable manifold trajectories for the multiple shooting method and the refined trajectory is indicated by the red line in Fig. 14(c). The total fuel consumption requested for this refined trajectory is 75.00 m/s. The TOF for the unstable segment ending at the insertion point around L_4 at $t_0=0.9T_S$ is 27.61 days and the TOF for the stable manifold segment and the patching segment in total is 165.01 days. The corresponding fuel consumption is 132.54 m/s and 1013.15 m/s, respectively. As shown in Fig. 14(a) and 14(b), by implementing the multiple shooting method at the second patching pair, only 8 loops are eliminated, corresponding to 147.99 days. Though the total TOF is not beneficial for fast transfers to L_4, the remaining loops around L_3 are not completely useless. For example, during its path from the Earth to L_4, a spacecraft can achieve 105.62 days flying around L_3 along the remaining loops serving for observation and communication purposes.

The trajectory design process at the third patching pair is similar to the first case, thus it is not discussed in detail. Details including the TOF and fuel consumption are listed in Table 3. The initial patching trajectory and the

refined trajectory are illustrated in Figs. 14(c) and 14(d), respectively.

So far, a construction method of Earth-Moon L_4 transfers leveraging the invariant manifolds of QPLO of L_3 is presented systematically in details and the sample transfer trajectories can be reproduced step by step following the aforementioned description.

Through the multiple shooting algorithm, most of the revolutions around L_3 can be eliminated (at least for the #1 and #3 patching pairs) but the quickest one among the example transfers still need 175.98 days to reach the L_4 vicinity. The patching examples demonstrate that the time encircling around L_3 is still dominant after patching and can not be further reduced in the frame of the current construction. Therefore, it enlightens the authors that if the multi-revolution behavior around L_3 can be completely avoided, a faster transfer may be achieved. Meanwhile, the results shown in Fig. 14(c) suggests that some stable manifolds alone can connect both the Earth vicinity and the L_4 vicinity without encircling around L_3 for many loops. In the next section, a new construction is explored and discussed.

Table 3 The TOF and fuel consumption for the selected patching pairs

# of the patching pair	Total TOF	Δv at perigee	Δv of the heteroclinic connection at patching pair	Insertion points near L_4	Δv at insertion points near L_4	Total Δv
1 (Fig. 13)	175.98 days	1494.85 m/s	69.51 m/s	$t_0=0.7T_S$	124.05 m/s	1688.41 m/s
				$t_0=0.8T_S$	118.92 m/s	1683.28 m/s
				$t_0=0.9T_S$	150.00 m/s	1714.36 m/s
2 (Fig. 14(a) and 14(b))	192.62 days	1013.15 m/s	75.00 m/s	$t_0=0$	102.48 m/s	1190.63 m/s
				$t_0=0.1T_S$	153.31 m/s	1241.46 m/s
				$t_0=0.9T_S$	132.54 m/s	1220.69 m/s
3 (Fig. 14(c) and 14(d))	177.37 days	1271.80 m/s	69.45 m/s	$t_0=0.2T_S$	173.70 m/s	1514.95 m/s
				$t_0=0.3T_S$	111.86 m/s	1453.11 m/s
				$t_0=0.4T_S$	150.45 m/s	1491.70 m/s
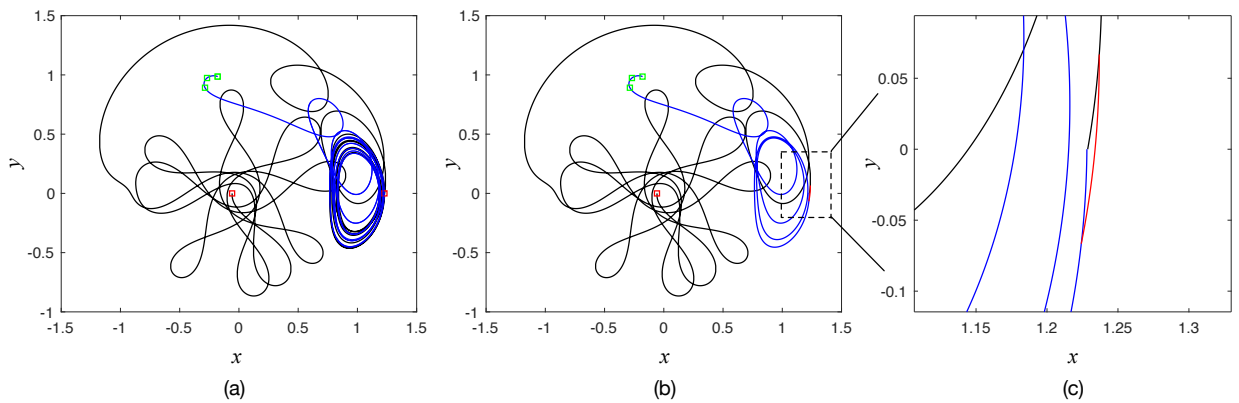
Fig. 13 The stable (black) and unstable (blue) manifolds segments corresponding to #1 patching pair in Fig. 12: the trajectories before (a) and after (b) multiple shooting method and a zoom-in version (c).
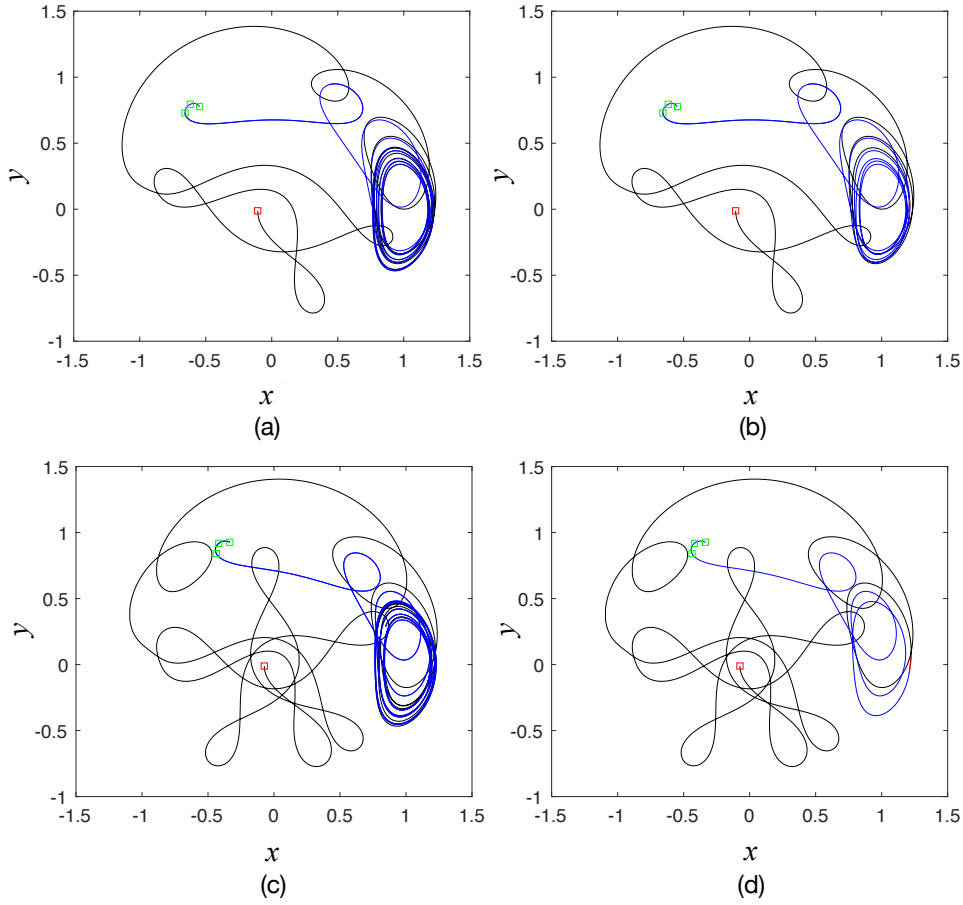
Fig. 14 The stable (black) and unstable (blue) manifolds segments corresponding to #2 and #3 patching pairs in Fig. 12: the trajectories before (a, c) and after (b, d) multiple shooting method.

4.3 Using Stable Manifolds Only

In the previous sections, the stable and unstable manifolds of the QPLO around L_3 are used to build up the transfer segments connecting the Earth and the L_4 vicinity, respectively. Through proper patching, the looping performances, including TOF, of the final trajectories can be adjusted by a combination of stable and unstable manifold segments from different initial conditions along the selected QPLO around L_3. However, Fig. 14(c) shows that stable manifold trajectories go very close to L_4 before they approach L_3 so it is possible to use solely the stable manifolds of the selected QPLO to construct L_4 transfer trajectories so that the looping around L_3 does not exist by such transfer trajectories. This section is devoted to the second construction of L_4 transfers by stable manifolds only.

As shown in **Section 3.1**, the performance of the stable manifolds of the specific QPLO around L_3 is examined by the sequence of Poincaré sections Σ_β and then picked out by whether the geometric condition that $r \in [r_{min}, r_{max}]$ is satisfied or not. Within the propagation time of 40 months backwards in time, the stable manifolds with perigee distance lower than 0.12 are chosen. The feasible stable manifolds connecting both the Earth and L_4 vicinity generate from the initial condition set

$U_3 = \{$#58, #65, #155, #316, #372, #660, #662, #670, #699, #760, #766, #816, #822, #851, #853, #862, #865, #872$\}$,

in the selected quasi-periodic Lyapunov orbit of L_3. There are several perigees along each of the feasible stable

manifolds trajectories, e.g., #862 stable segment approaches the Earth at 19 different perigees with their perigee distance ranging from 0.02 to 0.11 and fuel consumption varying from 1.0 km/s to 1.96 km/s, as shown in Fig. 15(a). Compared with the results in **Section 3.2**, the maximum fuel consumption at perigee in this case is lowered from 2.85 km/s to 1.96 km/s and less transfer opportunities are gained by the second construction using stable manifolds only.

Fig. 15(b) illustrates the distribution of TOF of feasible stable manifold trajectories from the Earth parking orbits to the insertion points near L_4. The TOF of all feasible stable manifolds varies from 60.86 days to over 757.78 days. In this case, both the minimum and maximum value of TOF is greatly decreased compared to the results shown in Fig. 9. Quicker transfers are obtained by solely stable manifolds because the looping behaviour around L_3 does not appear in this case. Furthermore, as shown in Fig. 15(b), perigees in the two black boxes lead to transit with total TOF shorter than 350 days from the Earth parking orbits with an altitude less than 0.05 to L_4 vicinity. These two black boxes correspond to #660 and #851 stable manifolds trajectories, with 4 and 16 perigees along them, respectively. Figs. 16(a) and 16(b) illustrate the L_4 transfers by #660 and #851 stable manifolds trajectories, where the perigee points and insertion points near L_4 are indicated by red and green squares, respectively. Along both trajectories, there are insertion points into the quasi-periodic orbits around L_4 at different t_0. The fuel consumption at these insertion points and the corresponding t_0 is listed in Table 4. The fuel consumptions at the insertion points near L_4 by the second construction is larger than the those by the first construction. The reason is that the effect of the Sun breaks the conservation of energy of the CR3BP and the Sun's cumulative effect during a longer transfer (e.g., the multi-revolution trajectory passing close to L_3) results in larger change in the fuel cost at the final insertion.

In summary, the second construction by solely stable manifolds owns an obvious advantage in the total TOF compared to the first construction method. However, the total number of perigee points along all feasible transfers is decreased from 970 in the case that both the stable and unstable manifolds (referred as the first case) are used, to 328 in the case of stable manifolds only (referred as the second case), which means that about 2/3 of the launch opportunities are lost. Importantly, a comparison on the set U_2 and U_3 shows that there are 64 feasible transfers in the first case but only 18 in the second case, about 3/4 of the transfers lost. Furthermore, as shown in **Section 4.2**, by the first construction, the looping TOF around L_3 can be adjusted and controlled by the multiple shooting method satisfying various mission requirements. Thus, another advantage of the first construction is that a designated looping around L_3 is achieved during the transfer from the Earth vicinity to L_4 vicinity, visiting and parking around two "high-cost" libration points far from the Earth in one transfer. The total fuel consumption is dominated by the cost switching from the circular Earth parking orbits to the stable manifold trajectories and determined by the altitude of the Earth parking orbit. A comparison of Fig. 15 and Fig. 7 shows that the minimum fuel consumption at perigee points in both cases is the same. Thus, it is hard to judge two cases on total fuel consumption.

**Table 4 The fuel consumption for selected stable manifolds trajectories**

# of the stable manifold	Δv at perigee	Insertion points near L_4	Δv at insertion points	Total Δv
#660 (Fig. 16(a))	1776.1 m/s - 1818.3 m/s	$t_0=0.1T_S$	196.61 m/s	1972.71 m/s - 2014.91 m/s

| | | $t_0=0.2T_S$ | 132.42 m/s | 1908.52 m/s - 1950.72 m/s |
| #851 (Fig. 16(b)) | 1709.0 m/s - 1810.1 m/s | $t_0=0.1T_S$ | 195.24 m/s | 1904.24 m/s - 2005.34 m/s |
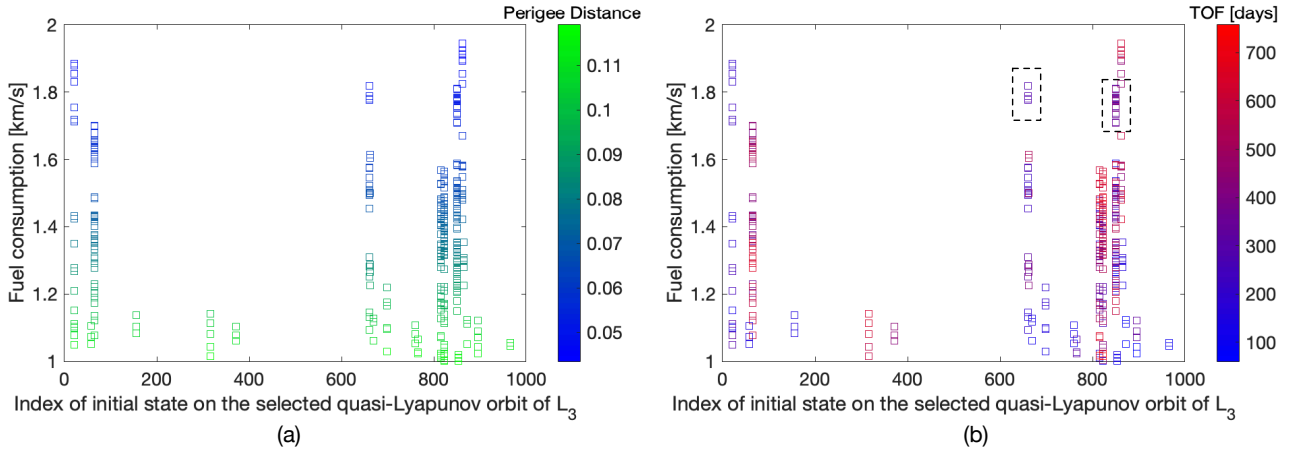
Fig. 15 The distribution of perigee distance (a) and TOF (b) of feasible stable manifolds generated from set U_3.
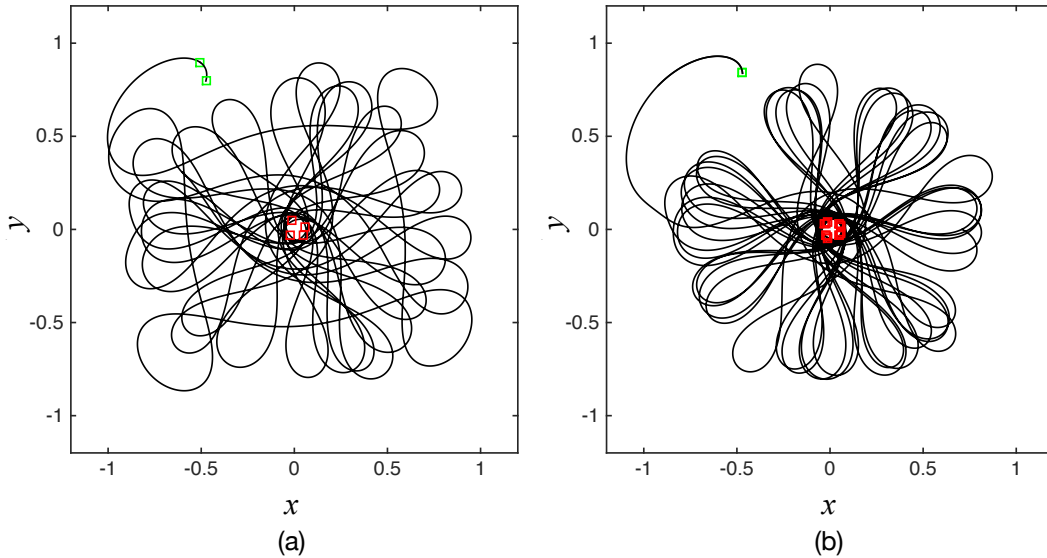
Fig. 16 Feasible transfer trajectories by solely stable manifolds #660(a) and #851(b): red squares indicate the perigees selected from Fig. 15(b); green squares indicate the insertion points to the neighborhood of L_4.

Conclusions

This paper is devoted to a new approach of transfers to the Earth-Moon triangular libration points in a Sun-Earth-Moon model via the stable and unstable manifolds of a quasi-periodic Lyapunov orbit (QPLO) around Earth-Moon L_3. The dynamics related to L_3 is used to achieve triangular libration point transfers for the first time.

Tentatively, the transfer segments from a circular Earth parking orbit to the L_3 vicinity and from the L_3 vicinity to quasi-periodic orbits around Earth-Moon L_4 are built up by stable and unstable manifolds of a selected QPLO of L_3, respectively. For that purpose, a three-level selection scheme is implemented. In the first level, with the

assistance of a sequence of Poincaré sections, unstable manifold trajectories passing through the quasi-periodic orbits around L_4 are selected geometrically, classified in a set called U_1. It is shown that among 1000 initial conditions along the chosen QPLO around L_3, 639 of them generate geometrical feasible unstable manifold trajectories and 177 with multiple intersection points. The range of the time of flight (TOF) from the L_3 vicinity to the L_4 vicinity is 55-69 days. These unstable manifold trajectories provide a sufficiently large set of feasible transfers connecting the L_3 vicinity to the L_4 vicinity for further selection in the third level.

In the second level, each trajectory in U_1 that approaches L_4 is associated to another stable manifold trajectory, so that they share the same (x, y) coordinates at a specific time. Then, the stable manifold trajectories are propagated to check their perigee distance within the maximum propagation time of 40 months. The initial condition set of feasible stable manifold trajectories is further narrowed to a set called U_2. Many of them own multiple perigees around the Earth, corresponding to multiple launch opportunities from the circular Earth parking orbits. Especially, one of them have 78 different perigees ranging from 0.02 to 0.11 in dimensional distance, covering the altitude of a 167 km low-parking orbit to a geostationary orbit. Their TOF ranges from 300 to 1000 days. To balance the TOF and altitude of the Earth parking orbits, the stable manifold trajectories connecting a circular Earth parking orbit of an altitude smaller than 0.04 and arriving at L_4 vicinity within 550 days are picked out. The total fuel consumption is dominant by the cost at the insertion from the stable manifolds to the Earth parking orbits, and thereby highly depends on the altitude of the target Earth parking orbits.

The third (and final) level is carried out to confirm that the corresponding unstable manifold trajectories in U_2 insert into a quasi-periodic orbit around L_4 at specific epoch $t_0=0, 0.1T_S, \ldots, 0.9T_S$. All members are confirmed to pass through the quasi-periodic orbits around L_4 at these moments but have different number of feasible insertion points. In the range from $0.1T_S$ to $0.6T_S$, there are more insertion points along all feasible unstable manifold trajectories. A quick calculation shows that the fuel consumption at all insertion points is less than 300 m/s, much smaller than the value at perigee points on the circular Earth parking orbits.

To control the total time of flight (TOF), the revolutions around L_3 are eliminated by patching the stable and unstable manifold segments generated from different points in the QPLO using the multiple shooting method. The range of the fuel consumption switching from the stable manifold segments to the unstable ones at the patching points is about 60-80 m/s. Thus, the fuel cost to fill the gap in this step can be regarded as a small correction compared to the dominant consumption at perigee points. Although one specific combination demonstrates that almost 12 loops around L_3 can be eliminated, saving 225.54 days, the quickest one among the example transfers still need 175.98 days to reach the L_4 vicinity.

In order to further reduce the TOF, the second construction using solely stable manifolds to transfer to the L_4 vicinity is explored through a similar selection scheme developed for the first construction. A large decrement in the total TOF is obtained and the lowest TOF is 60.86 days. However, the results also demonstrate that the second construction leads to much less transfer opportunities in the sense of number of transfer trajectories and launch opportunities from the Earth parking orbits. Two constructions show no advantage in total fuel consumption.

Acknowledgements

References

[1] V. Szebehely, Theory of orbit: The restricted problem of three Bodies, chap. 5, Academic Express, New York, 1967.

[2] C. Maccone, Planetary defense from the nearest 4 Lagrangian points plus RFI-free radioastronomy from the farside of the Moon: a unified vision, Acta Astronaut. 50 (2002) 185-199, https://doi.org/10.1016/S0094-5765(01)00176-X.

[3] Y. Liang, J. Shan, M. Xu, S. Xu, Capturing an asteroid via triangular libration points, J. Guid. Control. Dynam. 43 (2020) 1099-1113, https://doi.org/10.2514/1.G004614.

[4] H. Hirabayashi, H. Hirosawa, VSOP International Team, The VSOP mission: a general introduction and current overview, Adv. Space. Res. 26 (2000) 589-595, https://doi.org/10.1016/S0273-1177(99)01174-6.

[5] Z. Sodnik, C. Heese, P. Arapoglou, K. Schulz, I. Zayer, R. Daddato, European deep-space optical communication program, in: Proceedings of SPIE, 10524, Free-Space Laser Communication and Atmospheric Propagation XXX, 2018, https://doi.org/10.1117/12.2288943.

[6] L. Cassady, A. Kodys, E. Choueiri, A thrust stand for high-power steady-state plasma thrusters, in: 38th AIAA/ASME/SAE/ASEE Joint Propulsion Conference & Exhibit, 2002, https://doi.org/10.2514/6.2002-4118.

[7] K.A. Catlin, C. A. McLaughlin, Earth-Moon triangular libration point spacecraft formations, J. Spacecraft and Rockets, 44 (2007) 660-670, https://doi.org/10.2514/1.20152.

[8] F.J.T. Salazar, J.J. Masdemont, G. Gómez, E.E.N. Macau, O.C. Winter, Zero, minimum and maximum relative radial acceleration for planar formation flight dynamics near triangular libration points in the Earth-Moon system, Adv. Space. Res. 54 (2014) 1838-1857, https://doi.org/10.1016/j.asr.2014.07.018.

[9] F.J.T. Salazar, O.C. Winter, E.E.N. Macau, J.J. Masdemont, G. Gómez, Zero drift regions and control strategies to keep satellite in formation around triangular libration point in the restricted Sun-Earth-Moon scenario, Adv. Space. Res. 56 (2015) 1502-1518, https://doi.org/10.1016/j.asr.2015.07.001.

[10] X. Hou, L. Liu, J. Tang, Station-keeping of small amplitude motions around the collinear libration point in the real Earth-Moon system, Adv. Space. Res. 47 (2011) 1127-1134, https://doi.org/10.1016/j.asr.2010.12.005.

[11] Z. Zhang, X. Hou, Transfer orbits to the Earth-Moon triangular libration points, Adv. Space. Res. 55 (2015) 2899-2913, https://doi.org/10.1016/j.asr.2015.03.008.

[12] F.J.T. Salazar, E.E.N. Macau, O.C. Winter, Chaotic dynamics in a low-energy transfer strategy to the equilateral equilibrium points in the Earth-Moon system, Int. J. Bifurcation Chaos, 25 (2015) 1550077, https://doi.org/10.1142/S0218127415500777.

[13] H. Lei, B. Xu, Low-energy transfers to cislunar periodic orbits visiting triangular libration points, Commun. Nonlinear Sci. Numer. Sim. 54 (2018) 466-481, https://doi.org/10.1016/j.cnsns.2017.05.031.

[14] M. Vaquero, K.C. Howell, Leveraging resonant-orbit manifolds to design transfers between libration-point orbits, J. Guid. Control. Dynam. 37 (2014) 1143-1157, https://doi.org/10.2514/1.62230.

[15] M. Tan, K. Zhang, J. Wang, Single impulsive transfer to the Earth-Moon triangular point L_4 in a bicircular model, Commun. Nonlinear Sci. Numer. Sim. 82 (2020), 105074, https://doi.org/10.1016/j.cnsns.2019.105074.

[16] I. Elliot, Jr.C. Sullivan, N. Bosanac J.R. Stuart, F. Alibay, Designing low-thrust enabled trajectories for a heliophysics smallsat mission to Sun-Earth L_5, in: 29th AAS/AIAA Space Flight Mechanics Meeting, 2019, Hawaii, US.

[17] C.J. Sullivan, I. Elliott, N. Bosanac, F. Alibay, J.R. Stuart, Exploring the low-thrust trajectory design space for smallsat missions to the Sun-Earth triangular equilibrium points, in: 29th AAS/AIAA Space Flight Mechanics Meeting, 2019, Hawaii, US.

[18] X. He, Y. Liang, M. Xu, Y. Zheng, Low-thrust transfer to the Earth-Moon triangular libration point via horseshoe orbit, Acta Astronaut. 177 (2020) 111-121, https://doi.org/10.1016/j.actaastro.2020.07.014.

[19] H. Zeng, J. Zhang, Modeling low-thrust transfers between periodic orbits about five libration points: manifolds and hierarchical design, Acta Astronaut. 145 (2018) 408-423, https://doi.org/10.1016/j.actaastro.2018.01.035.

[20] O. Trivailo, Spacecraft stability, dynamics and control near the triangular Lagrange points influenced by multiple Trojan asteroids, Acta Astronaut. 60 (2007) 658-675, https://doi.org/10.1016/j.actaastro.2006.07.015.

[21] G. Gómez, C. Simó, J. Llibre, R. Martinez, Dynamics and Mission Design Near Libration Points: Volume II Fundamentals: The Case of Triangular Libration Points, World Scientific, Singapore, 2001, chap. 1.

[22] E.J. Doedel, V.A. Romanov, R.C. Paffenroth, H.B. Keller, D.J. Dichmann, J. Galán-Vioque, A. Vanderbauwhede, Elemental periodic orbits associated with the libration points in the circular restricted 3-body problem, Int. J. Bifurcation Chaos, 17 (2007) 2625-2677, https://doi.org/10.1142/S0218127407018671.

[23] Y. Liang, G. Gómez, J.J. Masdemont, M. Xu, Stable regions of motion around a binary asteroid system, J. Guid. Control. Dynam. 42 (2019) 2521-2531, https://doi.org/10.2514/1.G004217.

[24] C. Simó, P. Sousa-Silva, M. Terra, Practical stability domains near $L_{4,5}$ in the restricted three-body problem: some preliminary facts, Springer Proceedings in Mathematics & Statistics, Vol. 54, Springer, Heidelberg, 2013, https://doi.org/10.1007/978-3-642-38830-9_23.

[25] E. Barrabés, M. Ollé, Invariant manifolds of L_3 and horseshoe motion in the restricted three-body problem, Nonlinearity, 19 (2006) 2065-2089, https://doi.org/10.1088/0951-7715/19/9/004.

[26] A. G. Van Anderlecht, Tadpole orbits in the L_4/L_5 region: construction and links to other families of periodic orbits, Master Thesis, Purdue University, 2016.

[27] C. Simó, G. Gómez, À. Jorba, J.J. Masdemont, The bicircular model near the triangular libration points of the RTBP, From Newton to Chaos, edited by Roy A.E., Steves B.A., Vol. 336, Plenum Press, New York, 1995.

[28] À. Jorba, J. Villanueva, On the persistence of lower dimensional invariant tori under quasi-periodic perturbations, J. Nonlinear Sci., 7 (1997) 427-473, https://doi.org/10.1007/s003329900036.

[29] À. Jorba, A numerical study on the existence of stable motions near the triangular points of the real Earth-Moon system, a dynamical system approach to the existence of trojan motions, Astron. Astrophys. 364 (2000) 327-338.

[30] A. Deprit, A. Deprit-Bartholomé, Stability of the triangular Lagrangian points, Astron. J. 72 (1967) 173-179,

[31] C. Valente, L. Marino, G. Orecchini, Stability of the motion near L_4 equilateral Lagrangian point, Acta Astronaut. 46 (2000) 501-506, https://doi.org/10.1016/S0094-5765(00)00010-2.

[32] B.J. Falaye, S.H. Dong, K.J. Oyewumi, et al., Triangular libration points in the R3BP under combined effects of oblateness, radiation and power-law profile, Adv. Space. Res. 57 (2015) 189-201, https://doi.org/10.1016/j.asr.2015.10.030.

[33] G. Gómez, À. Jorba, J.J. Masdemont, C. Simó, Dynamics and Mission Design Near Libration Points: Volume III Advanced Methods for Collinear Points, World Scientific, Singapore, 2001, chap. 3.

[34] W.S. Koon, M.W. Lo, J.E. Marsden, S.D. Ross, Shoot the Moon, in: AAS/AIAA Astrodynamics Specialist Conference, 2000, Denver, US.

[35] À. Jorba, B. Nicolás, Transport and invariant manifolds near L_3 in the Earth-Moon bi-circular model, Commun. Nonlinear Sci. Numer. Sim. 89 (2020) 105327, https://doi.org/10.1016/j.cnsns.2020.105327.

[36] S. Huang, Very restricted four-body problem, NASA Technical Note, TN D-501, 1960.

[37] J. Cronin, P.B. Richards, L.H. Russell, Some periodic solutions of a four-body problem, Icarus, 3 (1964) 423-428, https://doi.org/10.1016/0019-1035(64)90003-X.

[38] E. Castellà, À. Jorba, On the vertical families of two-dimensional tori near the triangular points of the bicircular problem, Celest. Mech. Dynam. Astron. 76 (2000) 35-54, https://doi.org/10.1023/A:1008321605028.

[39] À. Jorba, Numerical computation of the normal behavior of invariant curves of n-dimensional maps, Nonlinearity, 14 (2001) 943-976.

[40] S.M. Lenz, H.G. Bock, J.P. Schlöder, E.A. Kostina, G. Gienger, G. Ziegler, Multiple shooting method for initial satellite orbit determination, J. Guid. Control. Dynam, 33 (2010) 1334-1346, https://doi.org/10.2514/1.48929.

[41] J. Sánchez, M. Net, On the multiple shooting continuation of periodic orbits by Newton-Krylov methods, Int. J. Bifurcation Chaos, 20 (2010) 43-61, https://doi.org/10.1142/S0218127410025399.

[42] G. Gómez, J. Llibre, R. Martinez, C. Simó, Dynamics and Mission Design Near Libration Points: Volume I Fundamentals: The Case of Collinear Libration Points, World Scientific, Singapore, 2001, chap. 1.1.4.

[43] J.S. Parker, K.E. Davis, G.H. Born, Chaining periodic three-body orbits in the Earth-Moon system, Acta Astronaut. 67 (2010) 623-638, https://doi.org/10.1016/j.actaastro.2010.04.003.

[44] Y. Liang, M. Xu, S. Xu, Low-energy weak stability boundary transfers to Pluto's moons: preliminary trajectory design via triangular libration point, Acta Astronaut. 156 (2019) 219-233, https://doi.org/10.1016/j.actaastro.2018.08.020.